Alba Tirado Bermúdez

Valorization of Forestry Derivatives into Functional Acrylic Polymers for Specific Applications

MASTER'S THESIS

Supervised by Dr. Adrian Moreno Guerra and Prof. Juan Carlos Ronda Bargalló

Master in Synthesis, Catalysis and Molecular Design

Analytical Chemistry and Organic Chemistry Department

UNIVERSITAT ROVIRA i VIRGILI

Tarragona

2023–2024

Acknowledgements

These last few months have been a new experience of which I am very proud to have been a part of. The knowledge I have gained, both academically and personally, has helped shape my identity and solidify my future academic and professional decisions. It is for these reasons, that I would like to express my gratitude to those who have supported me from the very beginning, because without them I would not have arrived until here.

First and foremost, I would like to thank my supervisors, Prof. Juan Carlos Ronda and Dr. Adrian Moreno, for their guidance, for sharing their knowledge and for giving me this opportunity. Additionally, I would like to show all my gratitude and appreciation to Prof. Virginia Cádiz, Prof. Marina Galià and Dr. Gerard Lligadas.

I would also like to extend my thanks to all the other members of the SUSPOL Research Group for their support and help both in and outside the laboratory. To Marc Palà and Javier Delgado, I strongly believe that this experience would not have been the same without you (and your terrible jokes). My gratitude also goes to Prof. Cristina Reguant and Dr. M. Isabel Araque for their help with the antibacterial trials.

Finalmente, me gustaría agradecer a mis amigos, mi familia y a Alex. Sin vuestro apoyo no hubiera podido llegar aquí. Gracias por siempre estar ahí incondicionalmente.

Abstract

The depletion of fossil resources and the growing environmental impact has led to the increase in interest and demand for sustainable and green materials. Consequently, much attention has been focused on integrating biomass as a renewable source of carbon to produce valuable-added chemicals and materials.

Towards this end, we have designed the preparation of a bio-based acrylate (HAAC4) through ring-opening aminolysis (ROA) of a bio-based cyclic lactone and a subsequent enzyme-catalyzed transesterification of the hydroxyamide precursor. Homopolymers were obtained through single electron transfer-living radical polymerization (SET-LRP) methodology, resulting in homopolyacrylates featuring tertiary amines. Kinetic experiments revealed characteristics of living radical polymerization (LRP) behavior, such as sustained propagation of radicals over time and near to perfect chain end functionality.

The synthesized monomers served as a major component in the preparation of sequential well-defined block copolymers (BCPs) composed of poly(butyl acrylate) (poly(BA)) and poly(HAAC4) segments, as hydrophobic and hydrophilic building blocks respectively. These amphiphilic copolymers demonstrated the ability to self-assemble in aqueous solutions, forming large compound micelles (LCMs) that have the potential to be used as surfactants stabilizers in emulsion polymerization of industrial relevant hydrophobic monomers such as styrene (S), thus providing a method for the preparation of stable latex dispersions. In addition, the monomer (HAAC4) could also be oxidized to the corresponding *N*-oxide acrylic analogue, that was employed in the preparation of antimicrobial hydrogels, showcasing the potential and versatility of HAAC4 for the preparation of advanced materials.

TABLE OF CONTENTS

LIST OF ACRONYMS AND ABBREVIATIONS

AA	Acrylic acid
ABCP	Amphiphilic block copolymer
ACH	Acetone Cyanohydrin
APS	Ammonium persulfate
ATRP	Atom transfer radical polymerization
BA	Butyl acrylate
BCP	Block Copolymer
CAC	Critical aggregation concentration
CALB	Candida antarctica lipase B
CVA	4,4'-azobis (4-cyanovaleric acid)
DCM	Dichloromethane
DI	Deionized
DLS	Dynamic light scattering
DMAPA	3-(Dimethylamino)-1-propylamine
DMSO	Dimethyl sulfoxide
DP	Degree of polymerization
DSC	Differential scanning calorimetry
DTGA	Derivative of thermogravimetric analysis
D_z	Hydrodynamic diameter
EBiB	Ethyl α-bromoisobutyrate
EBP	Ethyl 2-bromopropionate
FRP	Free radical polymerization
FU	Furfural
GBL	γ-Butyrolactone
GHSQC	Gradient heteronuclear single electron quantum coherence
HAAC4	4-((3-(Dimethylamino)propyl)amino)-4-oxobutyl acrylate
HAAC4-HGEL	4-((3-(Dimethylamino)propyl)amino)-4-oxobutyl acrylate-based hydrogel
HAC4	*N*-(3-(Dimethylamino)propyl)-4-hydroxybutanamide
ISET	Inner-sphere electron transfer
IZ	Inhibition zone
LCM	Large compound micelle
LRP	Living radical polymerization
MA	Methyl acrylate
MAA	Methacrylic acid
MBA	*N*, *N*'-Methylenebis(acrylamide)
MBP	Methyl 2-Bromopropionate
*m*CBA	3-Chlorobenzoic acid

*m*CPBA	3-Chloroperbenzoic acid
Me_6-TREN	Tris[2-(dimethylamino)ethyl]amine
MMA	Methyl methacrylate
M-S	Molecular sieves
MTBE	Methyl *tert*-butyl ether
MWD	Molecular weight distribution
NMP	Nitroxide mediated polymerization
NMR	Nuclear magnetic resonance
N-Ox-HAAC4	3-(4-(Acryloyoxy)butanamido)-*N*,*N*-dimethylpropan-1-amine oxide
N-OX-HAAC4-HGEL	3-(4-(Acryloyoxy)butanamido)-*N*,*N*-dimethylpropan-1-amine oxide-based hydrogel
OSET	Outer-sphere electron transfer
PBS	Phosphate-buffered saline
PDI	Polydispersity index
RAFT	Reversible addition-fragmentation polymerization
RDRP	Reversible deactivation radical polymerization
ROA	Ring-opening aminolysis
S	Styrene
SA	Succinic acid
SEC	Size exclusion chromatography
SET	Single electron transfer
SET-LRP	Single electron transfer-living radical polymerization
TBD	1,5,7-triazabicyclo[4.4.0]dec-5-ene
TEA	Triethylamine
TEM	Transmission electron micoscopy
T_g	Glass transition temperature
TGA	Thermogravimetric analysis
THF	Tetrahydrofuran
TMS	Tetramethylsilane
TREN	Tris(2-aminoethyl)amine

INTRODUCTION AND THEORETICAL BACKGROUND

The present Master's Thesis has been developed at the Organic Chemistry area of the Analytical Chemistry and Organic Chemistry Department from the Rovira i Virgili University, in the SUSPOL research group, which focuses on the development of advanced functional polymeric materials derived from renewable resources.

Motivation and state of the art

The industrial manufacture of various chemicals and commodity polymers is heavily dependent on fossil resources. Despite the dwindling of these non-renewable resources, coupled with alarming environmental impacts like global warming and waste accumulation, the demand for chemicals and materials reliant on petroleum has been on the rise. Growing awareness about these issues has begun to push society towards a greater demand for sustainable and green products.[1–3]

Polymers are the most widely produced synthetic consumer products globally, with annual production reaching 400 million metric tons in 2022.[4] The success of plastics as a material is inherently related to their range of outstanding and versatile properties such as light weight, low cost and easy processability, that makes them the material of choice for diverse applications, including packaging, construction materials, electronics, biomedical devices and energy storage among others.[5]

Among them, commodity polymers derived from (meth)acrylic monomers, (meth)acrylate polymers, are one of the most popular due to the wide range of monomers available to be polymerized, ranging from hydrophobic to hydrophilic, and the possibility to control their molecular weight and architectures through reversible deactivation radical polymerization (RDRP) methodologies.[6,7] Additionally, (meth)acrylate polymers are characterized for their interesting properties such as high glass transition temperatures (T_g) values (≥80 ºC), attractive mechanical properties, thermal stabilities and transparency which make them versatile for numerous applications.[8] Nevertheless, the vast majority of (meth)acrylate polymers available on the market are derived from petroleum-sourced resources and their production usually involves non-sustainable synthetic methodologies.[9] For example, poly(meth)acrylates are high valuable daily-life polymers commonly prepared from acrylic and methacrylic acids (AA and MAA) and their corresponding esters following strategies such as propylene oxidation[10] or the Acetone Cyanohydrin (ACH) process[11] which are far away in terms of environmentally friendly chemistry processes.

Over the last few decades, these concerns have led to biomass garnering significant attention as a renewable carbon feedstock for producing valuable chemicals, offering an alternative to those

derived from fossil resources. Owning to the importance of lignocellulosic biomass being the most abundant and bio-renewable resource on earth, great efforts have been directed towards developing new methods to produce bio-based value-added platform chemicals, and in this context a diverse palette of over 200 products is now available.[1–3]

Therefore, it is not surprisingly, that initial efforts have already been reported in the preparation of bio-based (meth)acrylate monomers, aimed at the subsequent production of sustainable and advanced polymeric materials using forestry biomass or carbohydrates as precursors.[12–14] However, bio-based water-soluble (meth)acrylate polymers are still largely unexplored despite their high demand in multiple applications such as surfactants, drug release or preparation of hydrogels.[15,16] Therefore, there is a clear need to not only formulate (meth)acrylic polymers derived from renewable resources but also to design chemical synthetic routes that reduce the reliance on toxic reagents and solvents during their preparation.

On this basis, γ-butyrolactone (GBL) is an interesting example of bio-based chemical that can be obtained from biomass. GBL, as depicted in Figure 1a, can be obtained via two primary pathways: through the 1,4-diacid platform as a transformation product of succinic acid (SA)[1], or through the xylose platform starting from furfural (FU).[17]

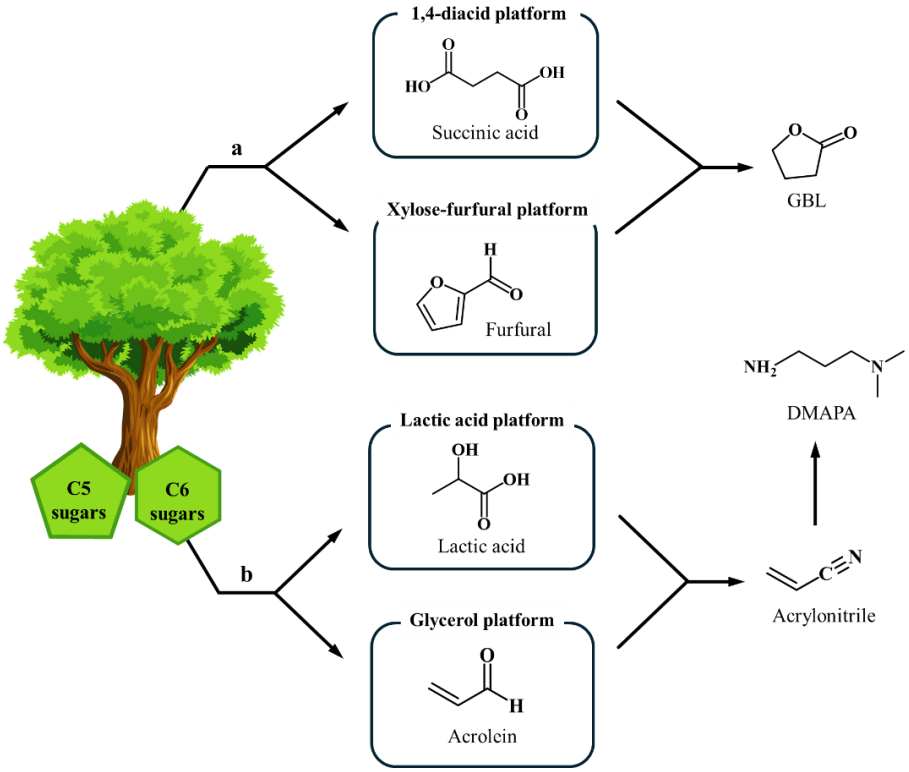

Figure 1. Routes for a) bio-based GBL and b) bio-based difunctional 3-(dimethylamino)-1-propylamine (DMAPA) starting from lignocellulosic C5 and C6 sugars.

GBL represents a unique platform for preparing bio-based acrylates through its direct transformation into the corresponding hydroxyamide via ring-opening aminolysis (ROA), followed by esterification to introduce the acrylate moiety. To incorporate tertiary amines as functional groups in the monomer structure, which would provide interesting properties such as water solubility and CO_2 interaction to the final polymer[18], 3-(dimethylamino)-1-propylamine (DMAPA) is a suitable nucleophile for this purpose. Currently, DMAPA is produced from fossil resources by reducing the aza-Michael addition of dimethylamine to acrylonitrile.[19] However, considering that green production routes for acrylonitrile have been described–such as from acrolein (a product of the glycerol platform) or through the lactic acid platform[20], as illustrated in Figure 1b, DMAPA can also be contemplated as a potential green product.

GBL and DMAPA-based acrylates offers the possibility to prepare *N*-oxide acrylate derivatives through the reaction of oxidant agents with tertiary amines. Polymeric materials containing *N*-oxide pendant groups are relevant for their distinct properties[21], including anti-fouling and antibacterial characteristics, which make them appealing for biomedical applications among others.[22]

Therefore, and taking into account the mentioned above state of the art, the present Master's Thesis aims to focus on the preparation of value-added polymers with tertiary amines and *N*-oxide pendant groups from GBL using simple and sustainable synthetic chemistry methods. To accomplish that, catalyst-free ROA of GBL employing DMAPA as a nucleophile will be studied, aiming to establish a robust method for the preparation of bio-based hydroxyamide. This hydroxyamide will then be converted into the corresponding bio-based acrylate monomers via enzymatic transesterification using methyl acrylate (MA) as the acyl donor. Subsequently, the polymerization behavior of this bio-based acrylate monomers will be also explored using RDRP methodologies to design amphiphilic block copolymers (ABCPs) and evaluate their potential as surfactants in emulsion polymerization. In addition, the obtained monomer will be also evaluated as precursor to access a *N*-oxide acrylate monomer and for the preparation of hydrogels with antimicrobial properties. Next sections will introduce the bases of the enzymatic esterification, RDRP methods employed and preparation of hydrogels since all are relevant in the context of this work.

Enzymatic esterification: towards the sustainable production of acrylate monomers

Acrylate esters are typically synthesized by reacting parent alcohols with acryloyl chloride, as displayed in Scheme 1a, involving toxic reagents and solvents such as dichloromethane (DCM), diethyl ether or tetrahydrofuran (THF) at room temperature.[23] This process requires the aid of a base such as triethylamine (TEA) to scavenge the hydrogen chloride (HCl) formed as result of

the nucleophilic acyl substitution. This reaction has low atom economy due to the production of TEA chlorhydrate which can be considered as a waste, requiring extensive washing to be eliminated affecting the final yield. Additionally, the method often results in brown resinous by-products, requiring purification by distillation or flash chromatography.

These challenges, combined with the aim of developing more sustainable synthetic methods, have led to considering the preparation of acrylates through transesterification with MA, which is presented in Scheme 1b. This process can be catalyzed by enzymes such as *Candida antarctica Lipase B* (CALB), producing methanol as the only by-product. In addition, the resulting acrylate monomers can be easily purified by simple filtration to remove the enzyme, followed by evaporation of the organic solvent and excess MA[24].

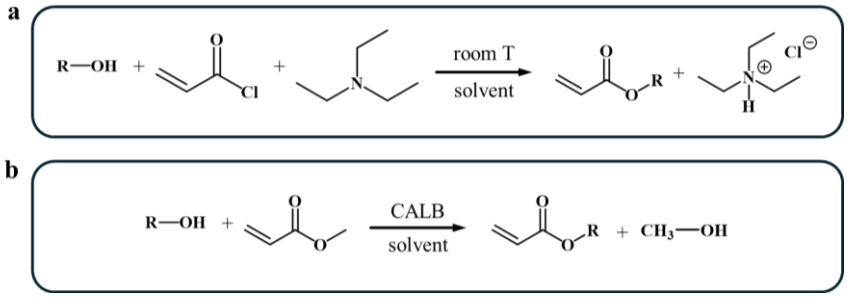

Scheme 1. a) Synthesis of acrylates from alcohols and acryloyl chloride via nucleophilic acyl substitution. b) Synthesis of acrylates from alcohols and MA via transesterification catalyzed by CALB.

In CALB-catalyzed transesterification, two type of acyl donors can be employed, which are represented in Scheme 2: alkyl esters and vinyl esters. With vinyl or isopropenyl esters, the reaction is irreversible due to the formation of an unstable enol that tautomerizes into the corresponding carbonyl compound. On the other hand, with alkyl esters like MA, the reaction is reversible and requires continuous removal of methanol to drive the reaction towards the product and maintain lipase activity, as methanol retention in the active site decreases catalytic efficiency.[25]

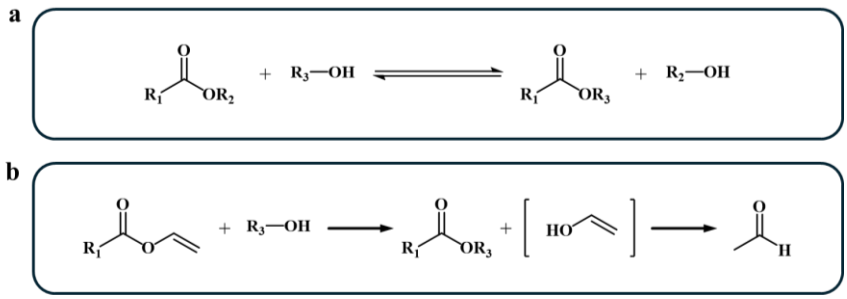

Scheme 2. Transesterification of esters with alcohols: a) reversible with an alkyl ester and b) irreversible with a vinyl ester.

Overall, CALB-mediated transesterification is a promising biocatalytic process conducted under mild, environmentally friendly and cost-effective conditions which offers high selectivity and activity towards a wide range of substrates, making it a versatile method for producing valuable products such as acrylate monomers, with potential applications in various fields.

Single Electron Transfer-Living Radical Polymerization (SET-LRP) as a RDRP method for the preparation of well-defined polymers.

Since its discovery in 2002,[26] SET-LRP has become a robust and versatile tool for synthesizing a wide range of vinyl polymers, including acrylates, methacrylates and acrylamides, with narrow molecular weight distributions (MWDs) (Đ<1.1) and high chain-end group fidelity. This allows for further *in situ* chain extensions and block copolymerizations, enabling access to complex architectures in a simple way.[27,28]

Compared to other RDRP such as nitroxide mediated polymerization (NMP), atom transfer radical polymerization (ATRP), and reversible addition-fragmentation polymerization (RAFT), SET-LRP stands out for its simplicity and ease of execution. This methodology is usually carried out under mild reaction conditions, at room temperature or below, uses a catalytic rather than a stoichiometric amount of catalyst, and allows using various combinations of monomers, initiators and solvents. The use Cu(0) as catalyst is another highlighting point, as it proves to be a robust and cost-effective catalyst compared to alternative methodologies that employ other types of catalyst such as air sensitive Cu(I). Its high tolerance to air, enables the utilization of commercial-grade monomers containing radical scavengers, and the simple purification required for the resulting polymers underscore the current success of this living radical polymerization (LRP) technique.[27–29]

SET-LRP, like ATRP, involves an equilibrium between active (propagating chains) and dormant (halide terminated chains) species.[30] The key difference between both relies in the activation step: SET-LRP uses zero-valent copper Cu(0) instead of Cu(I). In addition, in SET-LRP Cu(0) activates the alkyl halide through an heterolytic outer-sphere transfer (OSET) mechanism, wherein the outer sphere electron donor Cu(0) transfers an electron to the alkyl halide (R-X) resulting in a radical anion which degrades via stepwise or concerted pathways to generate $R\cdot$ and X^- allowing the propagation step.[29,31] In contrast, ATRP operates via an inner-sphere electron transfer (ISET) mechanism, involving the formation of the radical species and the deactivation species through a concerted homolytic halogen transfer between the halogen radical from the dormant species to active species.[31–33]

SET-LRP Mechanism

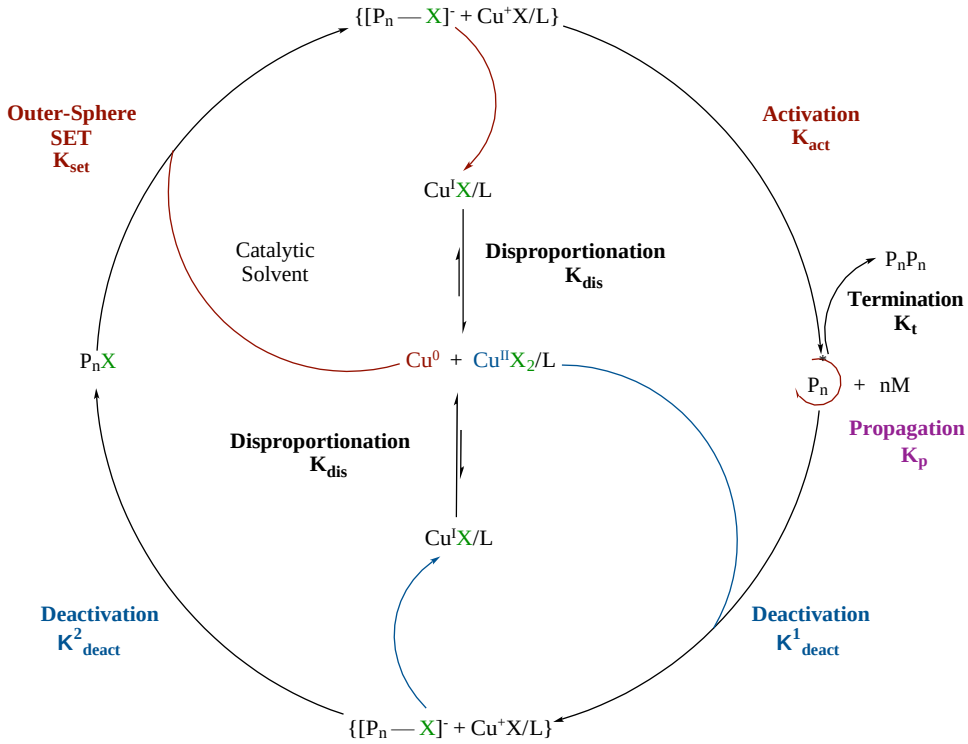

Scheme 3. SET-LRP mechanism adapted from reference 34.

The proposed mechanism for SET-LRP, presented in Scheme 3, involves four key steps. Initially, Cu(0) species act as electron donors, activating an alkyl halide initiator via stepwise or concerted single electron transfer (SET) process, which generates radicals through heterolytic bond cleavage. Next, the Cu(I)X/L, where L is a nitrogen-containing ligand, formed during radical generation, disproportionate *in situ* into highly reactive nascent Cu(0) and Cu(II) species that mediate the initiation and the reversible deactivation respectively. The third step involves the propagation phase, where monomers are added to the growing chain radicals. Finally, as the last step, the propagating radicals are homogenously deactivated by Cu(II)X_2L.

A crucial aspect of this mechanism is the self-regulated disproportionation of Cu(I)XL into Cu(0) activator and Cu(II)X_2L deactivator. Since Cu(0) serves as the catalyst, its regeneration *in situ* via disproportionation is essential for SET-LRP.[29] Poor disproportionation of Cu(I)X can lead to alternative polymerization mechanisms, resulting in polymers with poor chain-end functionality.[35,36] This disproportionation step is mediated in the presence of various solvents and *N*-containing ligands that destabilize Cu(I)X by preferentially binding to Cu(II)X_2, making the choice of both ligand and solvent crucial for an effective SET-LRP process.

The choice of an appropriate initiator is one of the key factors for effective control over polymerization. The initiator's activity must match the corresponding monomer to align the initiator radical's structure with the propagating chain.[37] As in other LRP techniques, the initiation rate must be faster than the propagation rate to produce well-defined polymers with narrow MWDs. Common monofunctional initiators for acrylate monomers, such as methyl 2-bromopropionate (MBP), ethyl α-bromoisobutyrate (EBiB) and ethyl 2-bromopropionate (EBP), which are represented in Figure 2, mimic the structure of polyacrylate growing species. Consequently, in the current work EBiB has been chosen as monofunctional initiator.

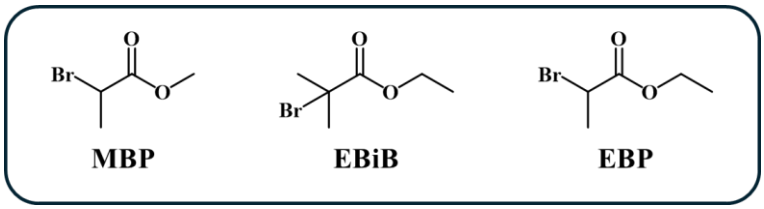

Figure 2. Representation of MBP, EBiB and EBP monofunctional initiators in SET-LRP.

Selecting the appropriate ligand is crucial in SET-LRP. Tris(2-aminoethyl)amine (TREN) and its methylated counterpart, tris[2-(dimethylamino)ethyl]amine (Me_6-TREN), illustrated in Figure 3, are commonly used because they effectively promote disproportionation through selective complex formation with Cu(II)X_2.[38] It is important to highlight that TREN provides slower rate of polymerizations than Me_6-TREN probably due to slower ability to promote the disproportionation step.[39] Taking this into account, Me_6-TREN was selected as ligand for SET-LRP experimentations carried out in this work. Ligand concentration is also a decisive parameter since high concentrations can induce termination by transferring a proton from the ligand to the polymer's bromine chain end.

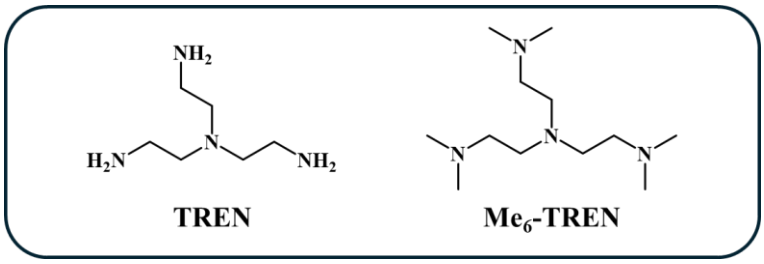

Figure 3. Representation of TREN and Me_6-TREN ligand in SET-LRP.

In SET-LRP, selecting the right solvent is also crucial. Beyond just dissolving the monomer and polymer, the solvent also can promote the disproportionation process -ensuring the high chain-end fidelity, and thus significantly impacting the polymerization process. SET-LRP is typically performed in a single phase, with DMSO and water being the most effective solvents due to their

high disproportionation constants. DMSO is considered the "holy grail" for SET-LRP as it facilitates rapid polymerization while maintaining control over molecular weight and polymer chain-end fidelity. This solvent promotes the SET process, since it mediates the rapid disproportionation of Cu(I)X and stabilizes Cu(0) nanoparticles, enhancing the polymerization rate.[40] Although DMSO is the most commonly used solvent, other solvents are also suitable for SET-LRP, as summarized in Figure 4, based on their ability to promote the disproportionation event.[41]

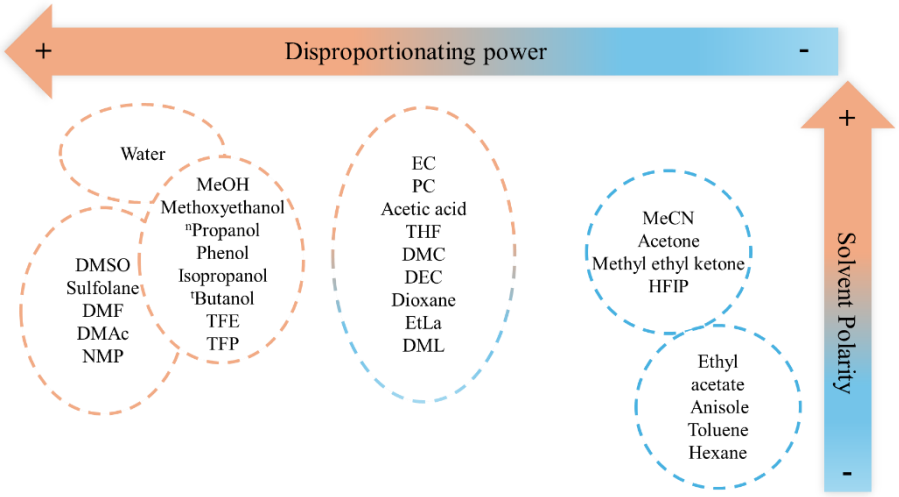

Figure 4. Solvent classification in function of their disproportionation ability and polarity adapted from reference 34. Blue circles indicate poor or non-disproportioning solvents, mixed orange-blue circles indicate moderate disproportioning solvents and orange circles represents good disproportioning solvents. (DEC: diethyl carbonate, DMAc: *N*, *N*-dimethylacetamide, DMC: dimethyl carbonate, DMF: *N*, *N*-dimethylformamide, DML: *N*, *N*-Dimethyl lactamide, DMSO: dimethyl sulfoxide, EC: ethylene carbonate, EtLa: ethyl lactate, HFIP: hexafluoroisopropanol, MeCN: acetonitrile, NMP: *N*-methylpyrrolidone, PC: propylene carbonate, TFE: 2, 2, 2-trifluoroethanol, TFP: 2, 2, 3, 3-tetrafluoro-1-propanol, TFH: tetrahydrofuran).

Here it is worth to mention, that the use binary mixtures of organic solvent and water is also possible, leading to biphasic SET-LRP systems. In the current work, DMSO and water were employed which allowed to combine the unique properties of both solvents to optimize the controlled radical polymerization processes.

Amphiphilic block copolymers for solution assembly applications

Amphiphilic molecules, or amphiphiles, are compounds that possess both hydrophilic (water-attracting) and hydrophobic (water-repelling) parts connected by covalent bonds within a single structure. Therefore, when amphiphiles are introduced into water, the molecules naturally aggregate due to their hydrophobicity regions, resulting in amphiphilic self-assembly into a wide

variety of structures including micelles, vesicles, nanotubes, nanofibers and lamellae.[42] Due to their amphiphilicity (or surface activity), the amphiphiles hydrophilic regions interact with water whereas the hydrophobic parts migrate to the interface. In this case the disruption of the cohesive energy at the interface favors a microphase separation between the selective solvent and the dispersed phase of the amphiphile, forming small closed interfaces or micelles-like aggregates.[43] The structure and the properties of the assemblies are deeply connected to the final architecture of the amphiphiles, providing opportunities for designing novel materials for advanced applications. Here it is important to mention, that the concept of amphiphilic self-assembly extends beyond small molecules to include macromolecules as well.[44]

Polymeric surfactants, or amphiphile-like polymers, consist of both hydrophilic and hydrophobic segments. Following the same principles as small-molecule amphiphile self-assembly, these polymers can form similar morphologies analogous to those of the small-molecule aggregates.[44] However, polymer aggregates exhibit higher stability and durability due to their mechanical and physical properties, making them appealing for a wide range of applications, such as biomedicine, biomaterials, micro-electronics and photoelectric materials among others.[14,44–47]

Advances in polymer synthesis have led to the development of numerous controlled polymerization techniques, such as LRP, enabling the preparation of polymers of various architectures, including block copolymers (BCPs), graft copolymers, dendritic polymers, star-like polymers and cyclic polymers. Among these, amphiphilic BCPs (ABCPs) are one of the most extensively studied system which consists of two immiscible blocks (i.e., different monomers used in the polymerization) that are covalently bound together and have a marked different solubility behavior. Owning to these different solubility properties, once in contact with water, they have the ability to form aggregates with different morphologies depending on the weight ratio of each block as depicted in Figure 5.

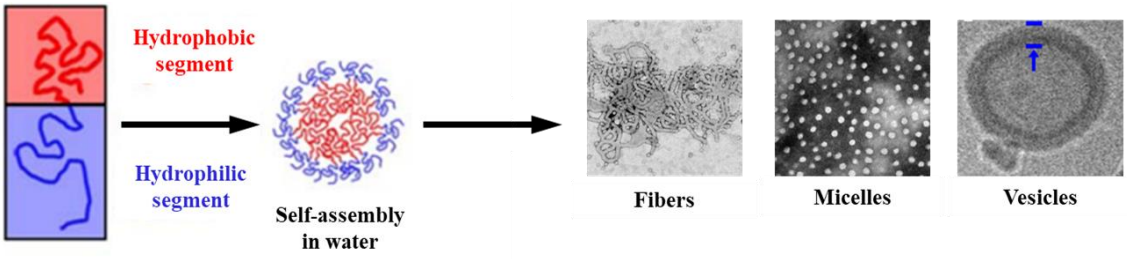

Figure 5. Representation of self-assembly of an amphiphilic AB polymer when dispersed in water and examples of some possible morphologies that can be obtained via careful tuning of the weight ratio of each monomer. TEM images (right) adapted from reference 14.

ABCPs have numerous applications, including their use as surfactants in emulsion polymerizations. In this context, the hydrophilic segments of the BCP provide colloidal stabilization to the polymer particles and confer specific surface functionalities, whereas the hydrophobic segments strongly adsorb or anchor to the polymer-water interface. The compatibility or miscibility between the hydrophobic block and the growing polymer particle is a very relevant parameter that determines how the ABCP is anchored to the particle surface, thereby impacting the stability and properties of the emulsion.[14,48,49]

Taking this into consideration, this work aims to synthesize well-defined BCPs using the previously introduced bio-based acrylate monomers as the hydrophilic and water-soluble segment in the BCP composition. The potential application of these BCPs as polymeric surfactants in the aqueous emulsion polymerization of relevant hydrophobic monomers such as styrene (S) and methyl methacrylate (MMA) will be investigated, providing a method for the preparation of stable latex dispersions.

Hydrogels: a promising material for biomedical and advanced technology applications

Hydrogels consist of cross-linked polymer-based three-dimensional networks of hydrophilic polymer chains (i.e., water-soluble polymers) that can absorb and swell in water, even reaching hundreds and thousands of times their dry weight without dissolving. This high-water adsorption ability is related to the presence of numerous hydrophilic functional groups such as -OH, -COOH, $-NH_2$ and $-SO_3H$, combined with a well-defined pore structure that becomes saturated with water.[50] Consequently, the swelling ability of hydrogels is heavily related to their potential applications in a wide range of fields, including biomedical, agriculture or energy sectors.[51–54] According to the cross-linking nature of the hydrogel, hydrogels, as illustrated in Figure 6, can be classified into chemically cross-linked hydrogels, physically cross-linked hydrogels and double interpenetrated network hydrogels.[54]

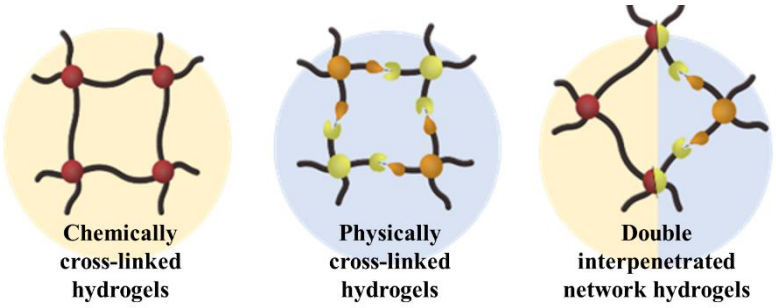

Figure 6. Schematic representation of the different types of hydrogels based on their cross-linking nature.

Hydrogels properties are closely tied to their crosslinking nature. Chemically cross-linking hydrogels are formed by covalent bonds, providing them with rigidity. One of the most popular

approaches for obtaining this type of hydrogels involves the thermal- or light- induced free radical polymerization (FRP) of water-soluble acrylic monomers in the presence of discrete cross-linking agents, which are small molecules with more than one reacting side such as *N*, *N*'-methylenebis(acrylamide) (MBA).[55] The high reactivity of both cross-linking agents and acrylic monomers usually imparts hydrogels with high mechanical properties but lacks repairability and elongation properties.[56] In the other hand, physical cross-linked hydrogels are based on non-covalent interactions such as hydrogen bonding, ionic interactions, van der Waals forces or hydrophobic interactions among others.[57] Therefore, the mechanical strength of this kind of hydrogels is based on polymer chain interactions.

The combination of both chemically and physically cross-linked hydrogels form the double interpenetrated network hydrogels, which combine both a strong covalent network with a flexible physical network to enhance toughness and strength under stress.[58]

Hydrogels find diverse applications across fields such as drug delivery, soft robotics, wound healing and flexible electronics among others.[55,59–61] However, finding new water-soluble acrylic monomer with inherent attractive functionalities remains a challenge, especially when it comes to the use of bio-based acrylic monomers. In this context and taking advantage of the water-soluble nature of the bio-based acrylic monomer prepared in this work, its transformation to the corresponding *N*-oxide zwitterion analogue will be explored with the ultimate objective of preparing *N*-oxide zwitterion-hydrogels with antimicrobial properties, potentially opening up the possibility of developing advanced functional materials.

OBJECTIVES

According to the state of art previously mentioned, the present Master's Thesis aims to synthesize and characterize bio-based an acrylic monomer derived from GBL and DMAPA and evaluate its potential oxidation to access *N*-oxide zwitterion bio-based acrylic monomers. In addition, it seeks also to explore the potential of the obtained monomers by preparing well-defined ABCPs through SET-LRP and hydrogels via free-radical polymerization (FRP), both with the aim of targeting relevant applications such as surfactants and antimicrobial coatings.

Towards this end, the following specific objectives have been planned and can be found displayed in Scheme 4:

- To obtain the targeted 4-hydroxyamide, *N*-(3-(dimethylamino)propyl)-4-hydroxybutanamide (HAC4), in bulk conditions and quantitative conversions following a catalyst-free ROA of GBL.
- To develop the aimed hydroxyamide acrylate, 4-((3-(dimethylamino)propyl)amino)-4-oxobutyl acrylate (HAAC4), via CALB mediated transesterification.
- To synthesize and characterize well-defined hydroxyamide polyacrylate (Poly(HAAC4)) via SET-LRP.
- To prepare and characterize well-defined ABCPs using a hydrophobic monomer butyl acrylate (BA) and as hydrophilic monomer the previously obtained hydroxyamide acrylate (HAAC4).
- To study the potential application of the ABCPs synthesized as macromolecular surfactant in the aqueous emulsion polymerization of industrial relevant hydrophobic monomers.
- To obtain and characterize the *N*-oxide zwitterion acrylate monomer through the oxidation of the previously prepared hydroxyamide acrylate (HAAC4).
- To develop a hydrogel based on the previously synthesized *N*-oxide zwitterion acrylate and to evaluate its antibacterial properties.

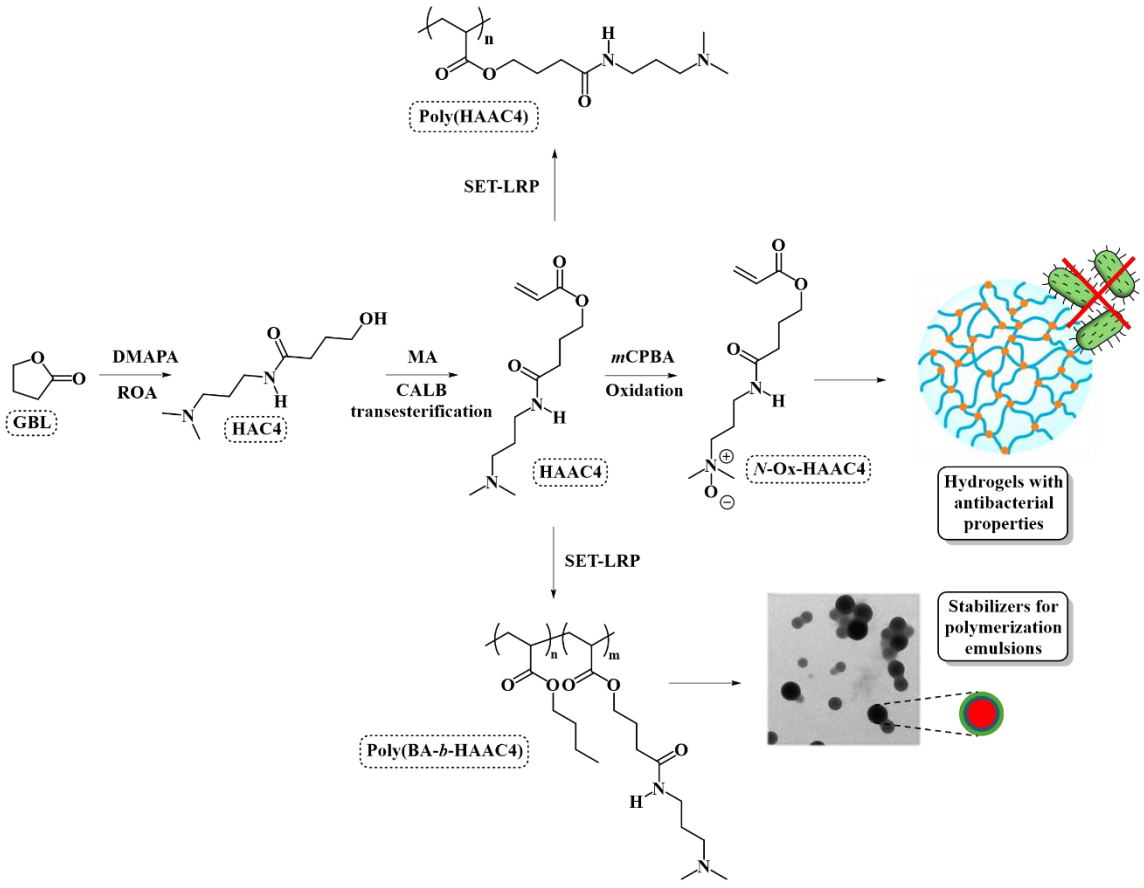

Scheme 4. Schematic representation of the different objectives of this work.

RESULTS AND DISCUSSION

Synthesis of bio-based hydroxyamide (HAC4)

As outlined in the introduction and the objectives, the first step involves the production of the targeted hydroxyamide from the bio-based lactone GBL while maximizing sustainable aspects in the synthetic process.

Albeit there are many synthetic methods to form amide linkages, most of them rely on activating a carboxylic acid using coupling agents, which results in undesired waste by-products. In contrast, directly converting an inactivated ester to an amide is a more efficient and straightforward process. Moreover, this method has a complete atom economy and avoids the formation of by-products since usually complete conversion is achieved.

Unlike their lower and higher homologs, five-membered lactones, or γ-lactones, exhibit low reactivity towards weak nucleophiles, such as water, due to the absence of ring and conformational strain. Because of this, γ-lactones do not experience ring-opening polymerization processes unless high pressures are used.[62]

However, when strong nucleophiles such as amines are employed with γ-lactones or δ-lactones, the reaction typically proceeds via acyl-oxygen cleavage through a bimolecular mechanism, resulting in the formation of the corresponding 4-hydroxyamide, as illustrated in Scheme 5a. In ring-strained lactones such as β-lactones, alkyl-oxygen cleavage can also occur, leading to the formation of the corresponding 3-aminoacid as by-product, as depicted in Scheme 5b.

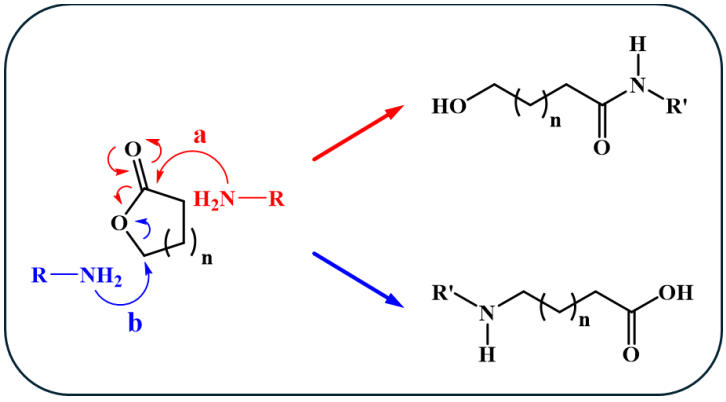

Scheme 5. Reaction pathways in the ring opening of lactones by nucleophiles.

In the literature, there are a plethora of synthetic protocols described for transforming inactivated esters or lactones into the corresponding amides, but many of them require stoichiometric amounts of harsh reagents like $AlMe_3$[63] or $LiNTf_2$[64]. In addition, numerous metal-based Lewis acids and organocatalysts have been effective in ester and lactone aminolysis. Notably,

1,5,7-triazabicyclo[4.4.0]dec-5-ene (TBD) has been proven effective in activating acyl moieties and is widely used in these transformations.[65]

To address sustainability issues, synthesizing GBL-derived hydroxyamides should ideally be performed under solventless and catalyst-free conditions, minimizing purification processes that usually lead to a decrease on the overall yield of the final product. The direct reaction of GBL with various amines generally leads to achieving high conversion with more nucleophilic primary amines. However, less reactive aromatic or secondary amines yield limited conversions unless high pressure or catalysts are employed.

In this work, ROA was performed following a catalyst-free bulk procedure with GBL and an slight excess of the targeted primary amine (molar ratio 1:1.05), DMAPA, at 60 ºC. The reaction is displayed in Scheme 6.

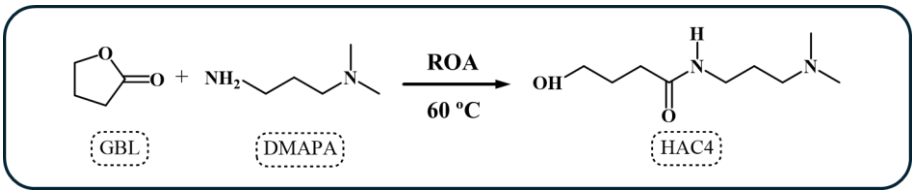

Scheme 6. ROA reaction of GBL with DMAPA.

This methodology enabled the multi-gram scale synthesis of the targeted 4-hydroxyamide, HAC4, which after removing under vacuum the slightly excess of DMAPA, was obtained as colorless oil in quantitative yield. In addition, the reaction proceeds in high-rate conversion, determined with kinetic experiments which are presented in Figure 7 and Figure S1, demonstrating that in fact only 3 h are needed to obtain high conversions values (≥98%). The obtained product was fully characterized by ^{1}H and ^{13}C nuclear magnetic resonance (NMR) spectroscopy, collected in Figure S2, as well as a gradient heteronuclear single electron quantum coherence (GHSQC) correlation spectrum, displayed in Figure S3.

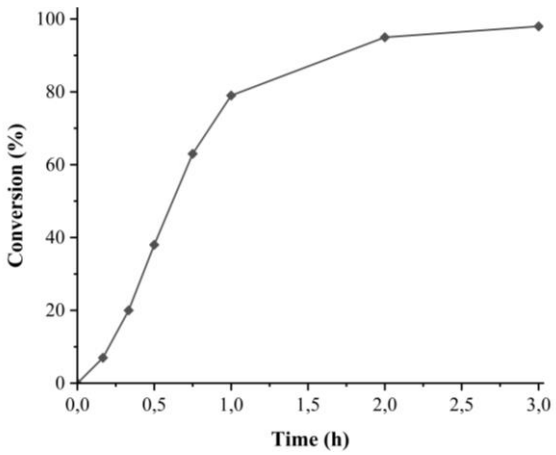

Figure 7. Kinetic plot for the ROA reaction of GBL and DMAPA at 60 ºC.

Synthesis of hydroxyamide acrylate (HAAC4) by CALB-mediated transesterification

Once prepared and characterized the HAC4 precursor, the next step was to introduce the acrylate functionality to obtain the target acrylic monomer.

CALB-mediated transesterification is a useful technique for synthesizing acrylic monomers.[24] This approach offers several advantages over traditional chemical methods, including milder reaction conditions, greater selectivity and higher yield values.

Lipase-catalyzed transacylation requires a non-polar, low-water environment to shift the thermodynamic equilibrium in favor of esterification and to prevent hydrolysis, so commercial CALB is typically dried before use.[66] For this reaction, preferred solvents are non-polar, such as hexane, toluene, isopropyl ether or methyl *tert*-butyl ether (MTBE). However, when the alcohol substrate possesses higher polarity, polar solvents such *tert*-butanol are required to ensure complete solubility. Due to the limited thermal stability of most lipases, including CALB, temperatures ranging from 40 ºC to 80 ºC are commonly employed.

Given these requirements, low-polarity (μ = 1.32 D; ε = 4.50) and low-boiling point (bp = 55.2 ºC) MTBE was chosen as the reaction media for this reaction. Since this is an equilibrium reaction, to shift the equilibrium towards the products an excess of MA (molar ratio 10:1) was used. The process remains sustainable independently of the large excess of MA employed, since it can be recovered alongside the solvent by fractional distillation after filtering out the CALB catalyst which allows to reuse both the catalyst and reaction media. In this work, 5 % (w/w) of CALB was employed, following established procedures. To continuously remove methanol and moisture, the

reaction was carried out under reflux using a Soxhlet device filled with freshly activated 4 Å molecular sieves (4 Å M-S), which is illustrated in Scheme 7.

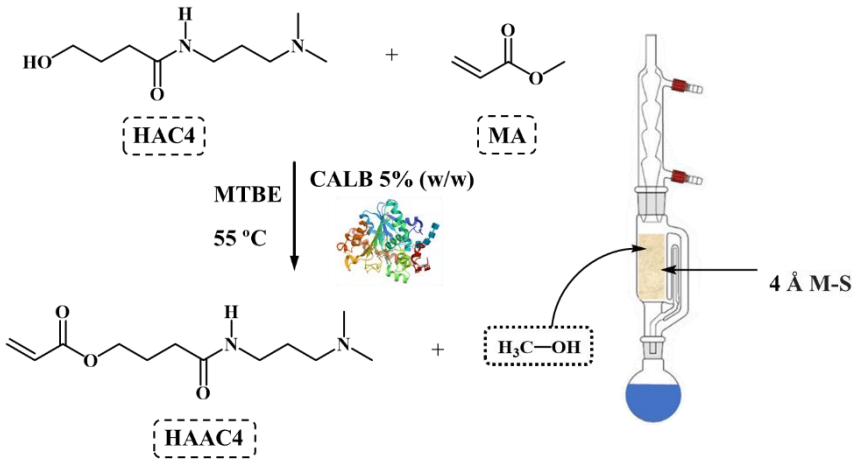

Scheme 7. Setting and conditions used in the CALB catalyzed transesterification of HAC4 with MA.

Prior to scaling-up the reaction, a kinetic experiment, collected in Figure 8 and Figure S4, was performed by measuring the conversion degree analyzing samples taken at preset times by ^{1}H NMR for the CALB-mediated transesterification reaction with HAC4 which indicated that the reaction proceeds smoothly reaching a complete conversion after 3 h.

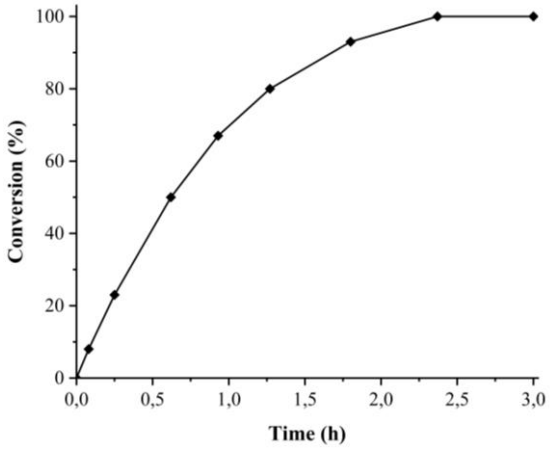

Figure 8. Kinetic plot for the CALB-mediated transesterification for the HAC4 precursor at 55 ºC.

Once the effectiveness of the transesterification method was confirmed under the employed conditions, the procedure was scaled up to 20.0 g to synthesize the target acrylate monomer, 4-((3-(dimethylamino)propyl)amino-4-oxobutyl acrylate (HAAC4) in large quantity. Complete conversion was achieved, and the product was isolated as a yellowish oil after a simple work-up which included removing CALB by filtration using Celite® and eliminating the excess of MTBE and MA under vacuum. The obtained product was fully characterized by ^{1}H and ^{13}C NMR

spectroscopy, collected in Figure S5, as well as a GHSQC correlation spectrum, displayed in Figure S6.

Cu(0)-Catalyzed SET-LRP of HAAC4

Polymerization of HAAC4 acrylate was investigated following SET-LRP as a RDRP methodology as illustrated in Scheme 8a. This technique is characterized for the use of Cu(0) as the reaction's catalyst. The goal of this experimentation was to determine if the polymerization of HAAC4 follows the main features of a controlled radical polymerization (CRP), which includes a constant and linear propagation of the radicals up to high monomer conversions accompanied with a controlled and narrow MWDs of the obtained polymer. In this case, the initiator selected was the tertiary α-haloester EBiB due to its electronic similarities with conventional acrylates.[37] Me_6-TREN was chosen as ligand due to its remarkable ability to promote the disproportionation even effectively via selective complex formation with Cu(II)X_2, providing a higher rate of polymerization than TREN which has a slower ability to promote the disproportionation step.[38,39] Dimethylsulfoxide (DMSO) (100 vol %) was chosen as solvent due to its high dipolar aprotic nature and its proved ability to promote the disproportionation of Cu(I)X in the presence of *N*-ligands and stabilizing Cu(0) nanoparticles[40], as already discussed in the introduction.

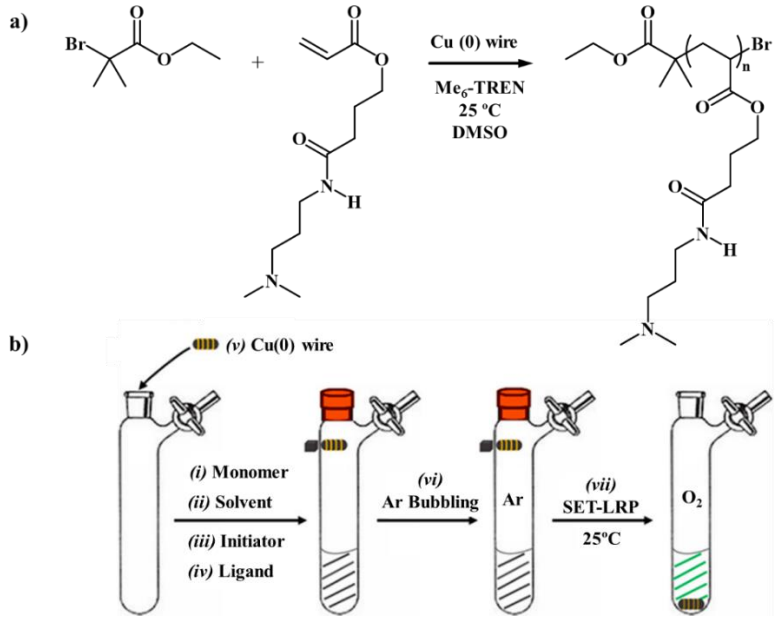

Scheme 8. a) Cu(0) wire-catalyzed SET-LRP of HAAC4 initiated with EBiB using Me_6-TREN as ligand in DMSO as solvent at 25 ºC. b) General procedure to perform Cu(0) wire-catalyzed SET-LRP in organic media. Adapted from reference 30.

The reaction protocol used in this work is depicted in Scheme 8b. When using Cu(0) wire as catalyst we proceed as follows: monomer, solvent, initiator, ligand and Cu(0) wire, which is usually wrapped around a stirring bar, are charged into a Schlenk flask. Importantly, the stirring bar is initially held above the reaction mixture using a small external magnet. Deoxygenation of the reaction mixture is accomplished by bubbling argon (Ar) for 15 min. To start the reaction, the stirring bar with the catalyst is gently dropped in, defining t = 0. The reaction is stopped by exposing the Schlenk flask to air. For kinetic experiments, a side arm of the tube is installed into the Schlenk flask and purged with Ar before removing two drops of the sample using an airtight syringe under the presence of a continuous Ar flow.

Before scaling up the reaction, kinetic measurement of the homopolymerization was performed. Figure 9a depicts the kinetic plot analysis for the polymerization using the monofunctional initiator EBiB at a targeted degree of polymerization (DP) of 50. ^{1}H NMR analysis of regularly withdrawn samples from the homogenous reaction mixtures was used to monitor monomer consumption during the reaction, represented in Figure S7. Unexpectedly, despite DMSO is ranked as a top solvent for SET-LRP, we observed that for the polymerization of the HAAC4 monomer the plot of ln([M]$_0$/[M]) versus times was linear only up to 75 min (76% conversion) ($K_p^{1\,app}$ = 0.016 min^{-1}), determined from the slope of the kinetic curve which is depicted in Figure 9a.

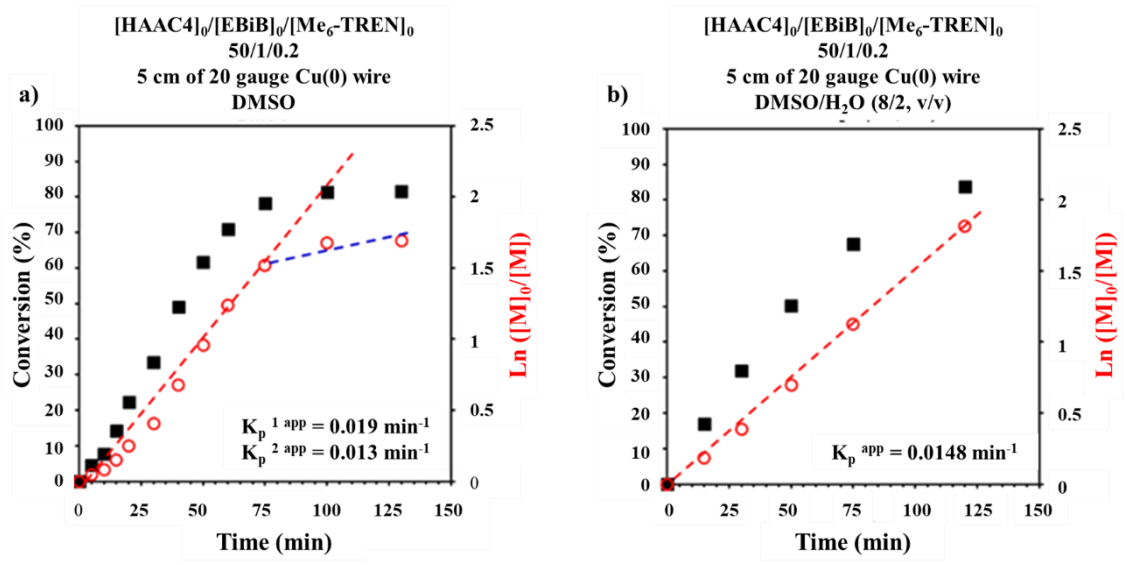

Figure 9. Kinetic plots for the SET-LRP of HAAC4 in a) DMSO and b) DMSO/water (8/2, v/v) mixtures initiated with EBiB and catalyzed by acid-activated Cu(0) wire at 25 ºC. The v/v ratio must be multiplied by 10 to obtain % solvent/% water. Reaction conditions; HAAC4 = 0.5 g; DMSO = 0.5 mL (a) and DMSO + water (0.5 mL). [HAAC4]$_0$/[EBiB]$_0$/[Me$_6$-TREN]$_0$=50/1/0.2.

These results indicate certain deficiencies in the disproportionation process in combination with a rapid activation, which lead to bimolecular termination events between growing chains. Another hypothesis is that the pendant tertiary amine of the monomer could coordinate with the generated $Cu(II)X_2$, interfering with the deactivation step or also induce termination by transferring a proton from the ligand to the polymer chain end. It has been previously reported that adding small amounts of H_2O to a non-efficient reaction mixture can significantly enhance its ability to produce reactive Cu(0) and the required levels of the $Cu(II)X_2$ deactivation to prevent irreversible chain termination in the early stages of SET-LRP reactions.[67] Moreover, DMSO and H_2O exhibit excellent synergy, achieving near-quantitative monomer conversion in biphasic SET-LRP systems.[68]

With the aim to improve control over the polymerization process, the kinetic experiments were repeated under the same conditions, but replacing DMSO as solvent for DMSO/H_2O (8/2, v/v) mixture. The kinetic plot obtained, illustrated in Figure 9b, revealed a linear rate constant of propagation of active species (K_p^{app} = 0.0148 min^{-1}) throughout the reaction, achieving high monomer conversions (90%) without a second kinetic regime. Therefore, the presence of 20% of H_2O in the reaction mixture was demonstrated to be essential for maintaining a constant propagation of the radicals over the entire polymerization process, minimizing bimolecular termination events.

Unfortunately, the MWD of the polymer at different monomer conversions (using the same samples from the kinetic experiments) by size exclusion chromatography (SEC), which is also crucial to verify the controlled behavior of the polymerization, could not be evaluated due to the high affinity of the poly(HAAC4) for the column stationary phase, as reported in the literature for similar polymers containing amino pendant groups.[69] Therefore, despite the insights gained from the kinetic polymerization experiments, it was not possible to solidly confirm the controlled radical polymerization of the HAAC4 monomer at this time.

However, analysis by ^{1}H NMR of poly(HAAC4), which was obtained as a yellowish viscous oil after being purified through dialysis against acetone to remove the remaining monomer, solvent and copper impurities at known monomer conversion and "programmed" DP = 50 allowed to determine the experimental molecular weight of the polymer. In this case, a sample with an 86% conversion was isolated and further analyzed by ^{1}H NMR. The relative integration of the signals corresponding to the end group (methyl substituents of the initiator) and the polymer were used to determine the experimental molecular weight, as shown in Figure 10. Since the experimental molecular weight and theoretical molecular weight were found to be very similar, it can be deduced that good control during the polymerization process was achieved with the introduction

of small amounts of water. Complete structural characterization of poly(HAAC4) by ^{1}H, ^{13}C NMR and GHSQC spectroscopy can be found in Figure S8 and Figure S9.

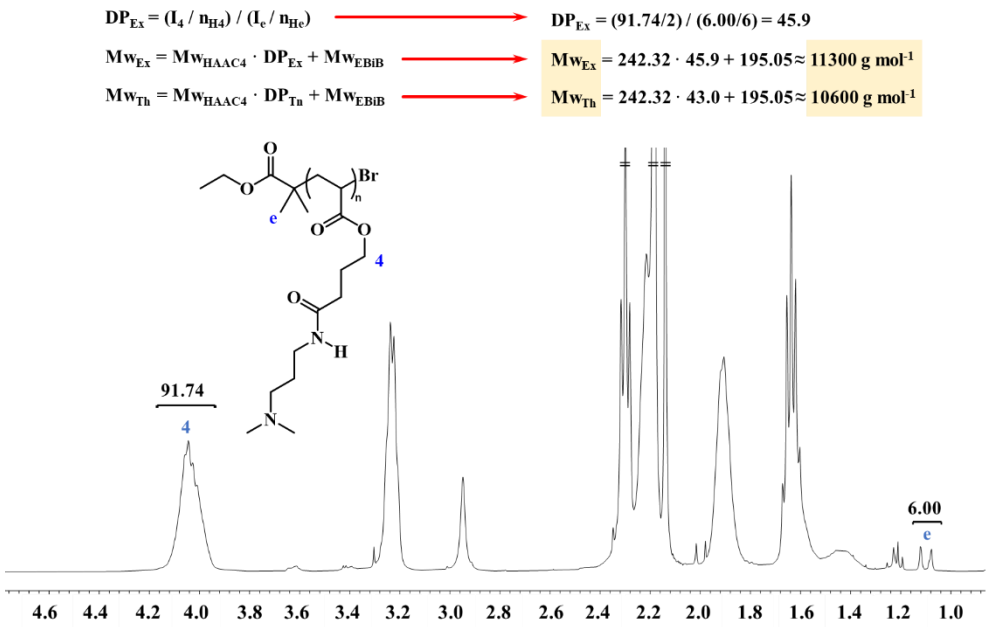

Figure 10. Determination of the molecular weight of poly(HAAC4) at 86% of monomer conversion obtained via SET-LRP in DMSO/water (8/2, v/v) as solvent, initiated with EBiB and using Me_6-TREN as ligand at 25 ºC.

The thermal properties of poly(HAAC4) were assessed by differential scanning calorimetry (DSC) and thermogravimetric analysis (TGA) techniques. DSC, illustrated in Figure S10, revealed a T_g for poly(HAAC4) at 2.5 ºC, consistent with its viscous, sticky state at room temperature. The polymer exhibited no melting events, confirming its amorphous nature. TGA analysis, collected in Figure S11a, showed thermal stability below 240 ºC, with a $T_{5\%}$ value of 258 ºC. Derivative of TGA (DTGA), shown in Figure S11b, plot indicated three main degradation steps: the primary degradation step (282 ºC) that could involve the ester cleavage, while the subsequent steps (at 346 ºC and 428 ºC) might correspond to amide cleavage and polymeric chain scission, respectively.

Synthesis amphiphilic block copolymers via Cu(0)-Catalyzed SET-LRP using HAAC4 as hydrophilic segment

Since the homopolymerization of HAAC4 was shown to be controlled with highly chain end fidelity, as confirmed by ^{1}H NMR spectroscopy studies, numerous opportunities for synthesizing more complex architectures are now unlocked. Given the fact that HAAC4 is a hydrophilic and water-soluble monomer, it provides an opportunity to combine it with hydrophobic, water-insoluble monomers to create ABCPs with different potential applications.

Among the many available hydrophobic monomers, butyl acrylate (BA) stands out as one of the most important, with numerous industrial applications such as dispersant component in paint industry.[70] Although different routes can be followed to produce BA, it is usually obtained from an equilibrium-limited esterification between AA and n-butanol over an acid cation exchanger catalyst, as represented in Scheme 9, followed by several distillation processes to extract BA from the organic phases.[71] However, bio-based BA can also be synthesized from butanol and AA, both chemicals that can be obtained from carbohydrate fermentation offering a more sustainable alternative to its petroleum-based counterpart.[72,73]

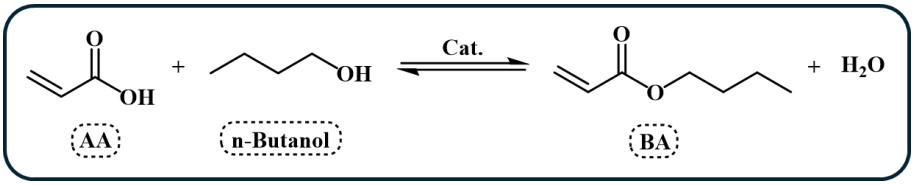

Scheme 9. Reaction scheme of the esterification of AA and n-butanol.

Therefore, the different water-solubility of the corresponding homopolymers, poly(HAAC4) being hydrophilic and water-soluble and poly(BA) being hydrophobic and water-insoluble-sparked our interest in studying the preparation of ABCPs and evaluate their ability to undergo self-assembly upon contact with aqueous solutions.

For the synthesis of the ABPCs composed of BA and HAAC4, a sequential monomer addition strategy was followed (i.e., *in situ* chain extension), in which after the polymerization of the first monomer at near to quantitative conversion -generation of the first block- the second monomer is added to continue the chain growth -generation of the second block- and produce the BCP, as illustrated in Scheme 10a. To ensure the successful preparation of the BCPs, BA was chosen as the first monomer to be polymerized due to its ability to efficiently initiate the polymerization of the second monomer, as depicted in Scheme 10a.

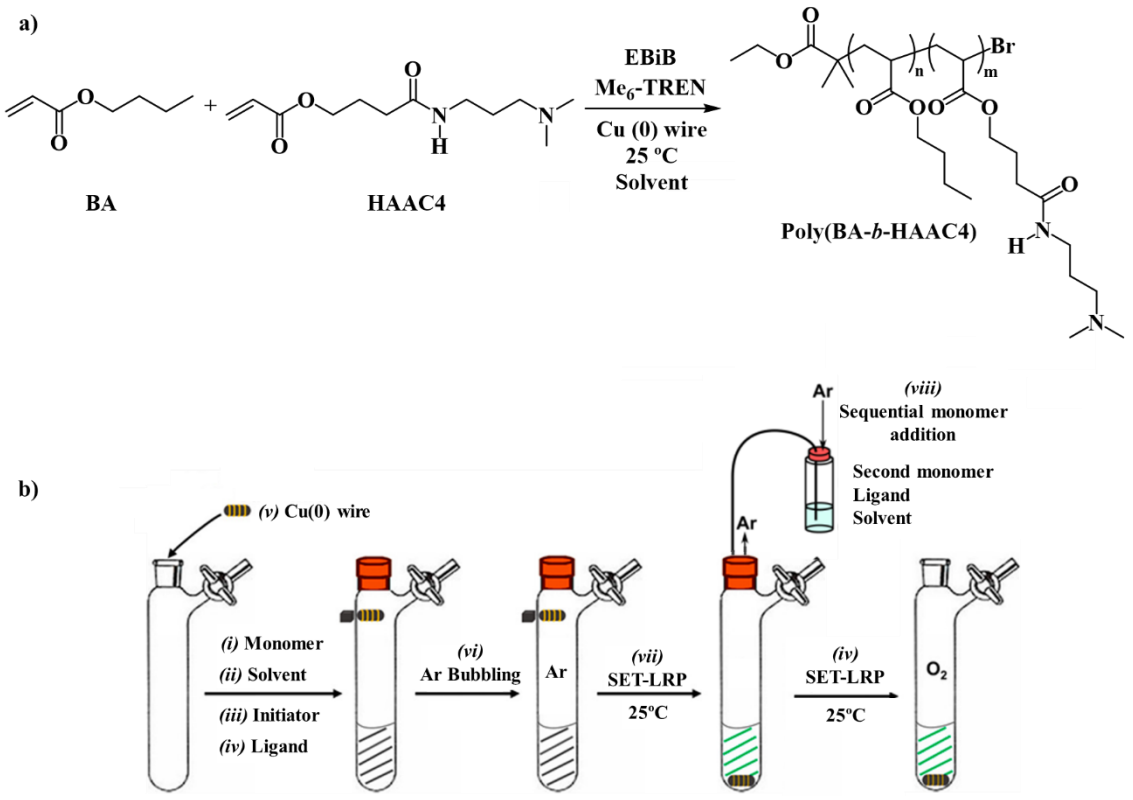

Scheme 10. a) Cu(0) wire-catalyzed SET-LRP of copolymerization of BA and HAAC4 initiated with EBiB using Me_6-TREN as ligand and DMSO as solvent at 25 ºC. b) General procedure to perform Cu(0) wire-catalyzed SET-LRP copolymerization in organic media. Adapted from reference 30.

The reaction protocol used for this reaction, as depicted in Scheme 10b, is similar to the homopolymerization SET-LRP procedure with the difference of the incorporation of the second monomer after near quantitative conversion of the first monomer alongside with the corresponding ligand and solvent.

In this case, since the final purpose of these copolymers were to explore the possibility to form nanoassemblies upon contact with water, initially BCPs were synthesized with a hydrophobic/hydrophilic ratio of 50/50 (mol/mol) to favor the formation of spherical micelles. First, the hydrophobic core block was synthesized by SET-LRP under conditions $[BA]_0/[EBiB]_0/[Me_6\text{-TREN}]_0$ = 50/1/0.2. Complete BA conversion was achieved in 2 hours, which enabled the *in situ* chain extension with HAAC4 (DP = 50) in the second step to produce poly(BA-*b*-HAAC4). The addition of small amounts of water (20 wt%) as in the case of the homopolymerization, was proven to be crucial for the preparation of poly(BA-*b*-HAAC4) since higher conversion values of HAAC4 were achieved whenever the biphasic system was employed (72%) instead of only DMSO as solvent (67%), as depicted in Figure 11. However, it was not

possible to acquire a hydrophobic/hydrophilic ratio of 50/50 (mol/mol), having achieved in the best result a hydrophobic/hydrophilic ratio of 50/36 (mol/mol).

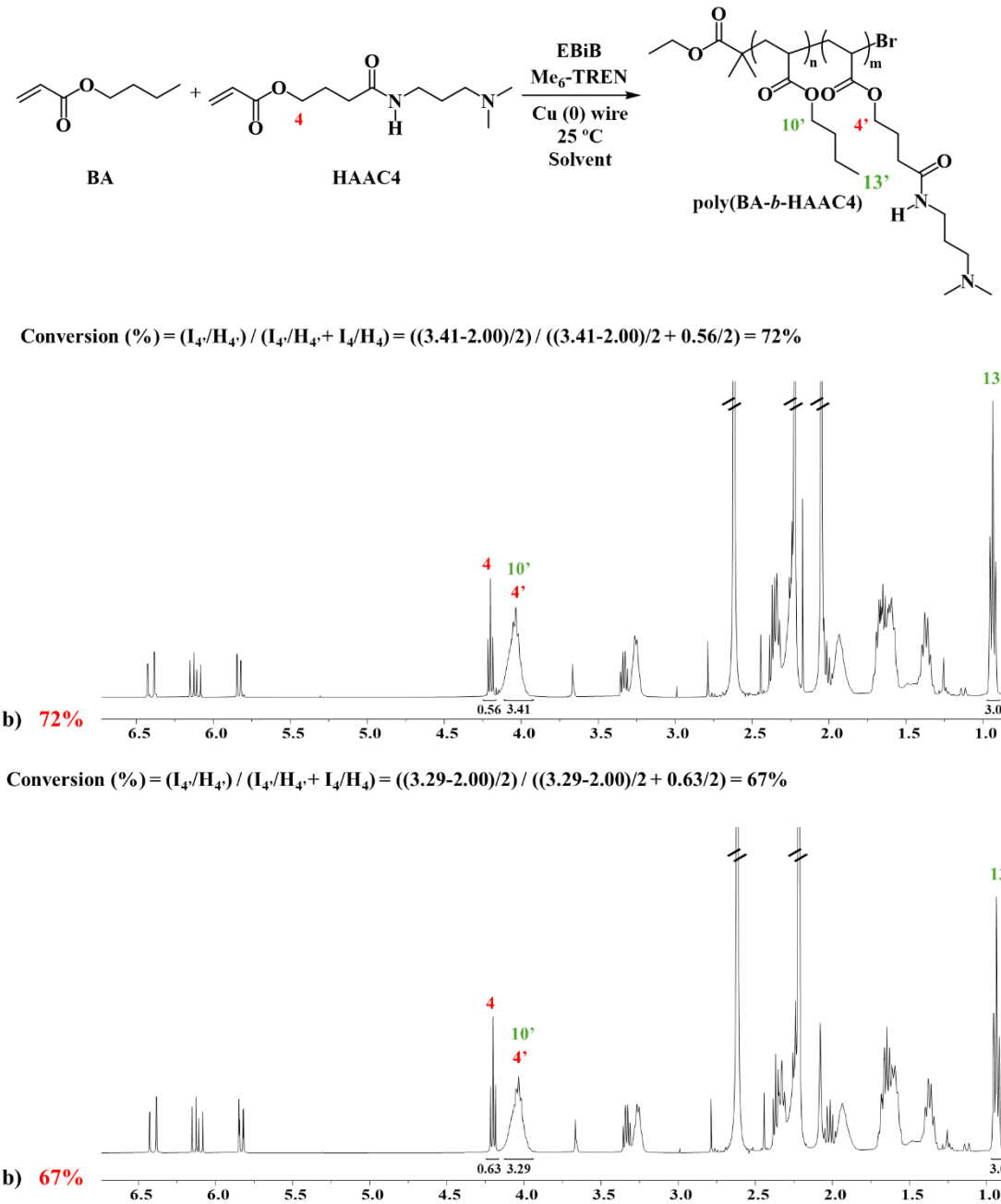

Figure 11. Superposed ^{1}H NMR spectra of HAAC4 and the reaction mixture prepared using as solvent a) DMSO and b) DMSO and H_2O (8/2, v/v) in the SET-LRP reaction after 24 h at 25 ºC.

Characterization by ^{1}H and ^{13}H NMR spectroscopy, collected in Figure S12, and GHSQC correlation spectrum, displayed in Figure S13 were performed and confirm the obtention of the BCP which was found to be a yellowish viscous oil after being purified through dialysis against acetone to remove the remaining monomer, solvent and copper impurities.

The thermal properties of poly(BA-*b*-HAAC4) were studied by DSC and TGA techniques. DSC, illustrated in Figure S14, revealed a unique T_g value for poly(BA-*b*-HAAC4) of -11.9 ºC, which correlates with the sticky and viscous nature of the copolymer at room temperature and indicated complete miscibility between both blocks. As expected, the polymer exhibited no melting points, due to its amorphous nature. TGA analysis, collected in Figure S15a, showed thermal stability below 250 ºC, with a $T_{5\%}$ value of 263 ºC. DTGA, shown in Figure S15b, indicated two main degradation steps: the primary degradation step (217 ºC) could be associated to ester cleavage linkages, while the subsequent broad step (403 ºC) could correspond to amide moiety cleavage and polymeric chain scission. In this case, only two degradation steps can be seen probably due to the more sophisticated architecture of the copolymer in contrast to the homopolymers.

General emulsion polymerization procedure using poly(BA-*b*-HAAC4) as stabilizer

Once copolymerization has been achieved, the next step was to study the self-assembly ability of the poly(BA-*b*-HAAC4). As previously mentioned in the introduction section, the two immiscible blocks that compose the final copolymer exhibit significantly different affinity behaviors. When in contact with water, these differences could trigger the blocks to form aggregates with various morphologies, depending on the weight ratio of each block.

The self-assembly of the copolymer was induced by adding water to a poly(BA-*b*-HAAC4) acetone solution dropwise while stirring (i.e., solvent exchange methodology) obtaining a solution with a final concentration of 5 g L^{-1}, represented in Figure 12a. A cloudy solution was obtained, indicating the formation of aggregates. The z-average hydrodynamic size (D_z) and morphologies of the self-assembled structures were further investigated by dynamic light scattering (DLS) and transmission electron microscopy (TEM). DLS analysis, represented in Figure 12b, revealed an average size of 269 nm with a dispersity of 0.5501 for the nanoparticles. However, two distinct populations were observed: one with a smaller size (~ 40 nm) and another with a larger size (~ 265 nm). In this case, the average size was significantly larger than the expected for single spherical micelles (~ 20-35 nm). The larger size could likely be a result from further aggregation of simple spherical micelles due to the existence of secondary interactions leading to large compound micelles (LCMs). These attractive interactions may be promoted by interactions such as hydrogen bonding. TEM analysis, showcased in Figure 12c, confirmed the presence of two different populations: smaller particles (~35 nm) and larger clustered particles (~160 nm). Therefore, these findings are consistent with the DLS measurements. Additionally, it can be observed that the particles do not present a smooth sphere-like structure, which could be attributed to the different hydrophobic/hydrophilic ratio of 50/36 (mol/mol) in the final copolymer, rather than the ideal 50/50 (mol/mol) ratio. Overall, these results demonstrate that poly(BA-*b*-HAAC4)

amphiphilic copoplymer can self-assemble into LCMs and open-up their potential application in different sectors such as surfactants or drug release.

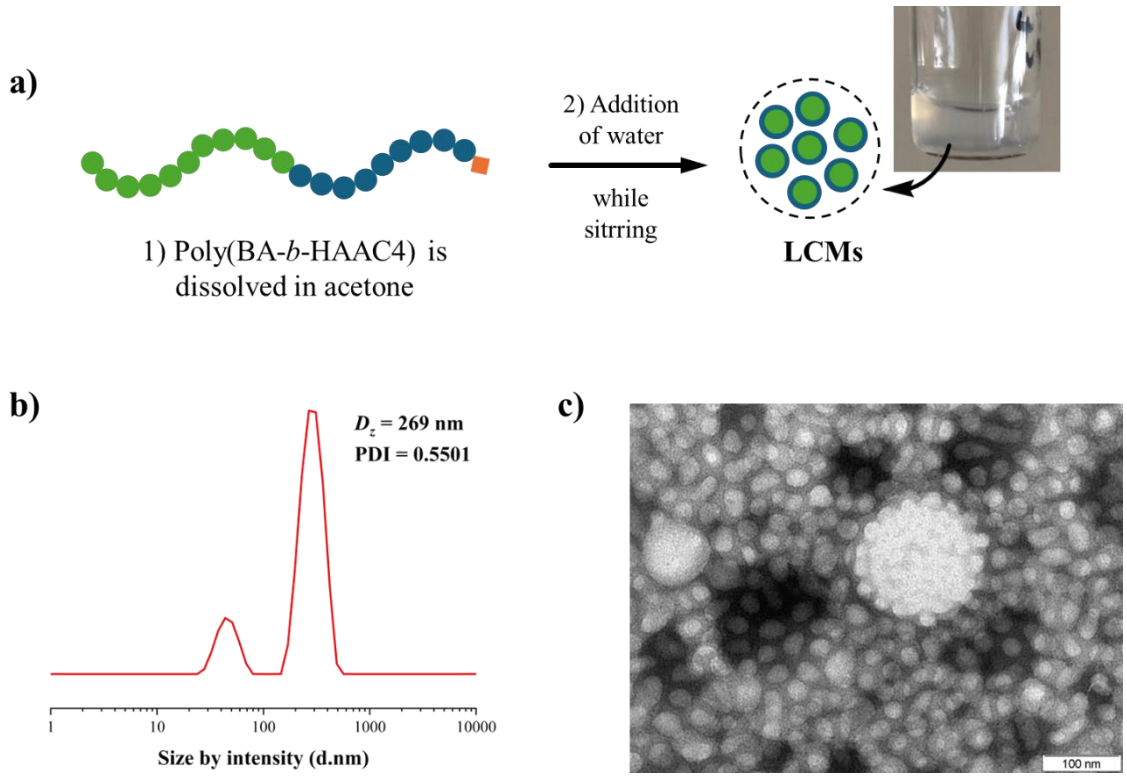

Figure 12. a) Schematic representation of the aggregates formation of poly(BA-*b*-HAAC4) upon contact in water. b) DLS size distribution by intensity of poly(BA-*b*-HAAC4) self-aggregates c) TEM image of the poly(BA-*b*-HAAC4) LCMs (scale bar is 100 nm).

Aqueous emulsion radical polymerization processes are highly relevant in the large-scale industrial synthesis of vinyl polymers.[74] Typically, a basic emulsion polymerization system includes a monomer or a mixture of monomers dispersed in water with the aid of a surfactant. While low-molecular-weight, short-chain stabilizers are commonly used, employing ABCPs as surfactants offers several advantages. These ABCPs surfactants possess unique properties in aqueous solutions, such as a low critical aggregation concentration (CAC) and a low diffusion coefficient, which enhance the properties of the resulting emulsion compared to conversional low-molecular-weight surfactants.[75,76]

Considering this, the FRP of emulsions composed of both S or MMA were conducted using 15 wt% of poly(BA-*b*-HAAC4) relative to the monomer as surfactant stabilizer, and 4,4'-azobis (4-cyanovaleric acid) (CVA) as the initiator, due to being partially water soluble and having an appropriate dissociation temperature (above room temperature), at 65 ºC for 4 hours, as schematized in Figure 13a. Under these conditions, poly(BA-*b*-HAAC4) proved be an efficient

stabilizer as no coagulum was observed during the polymerization and stable latex dispersions could be obtained regardless the monomer employed. Under the described conditions, high conversion rates were obtained for both emulsions: 75% for the poly(S) emulsion and 91% for the poly(MMA) emulsion. DLS analysis, showcased in Figure 13b and Figure 13d, revealed a broad large-sized particle population in the latex dispersions of both monomers, as well as a small population at bigger size which could correspond to minimum percentage of sedimentation since samples were not pre-processed. The average D_z for poly(S)-latex particles was found to be larger than that of poly(MMA)-latex particles (235 nm vs 198 nm). TEM analysis, collected in Figure 13c and Figure 13e, confirmed the presence of different sizes of spherical latex particles in both experimentations, which correlates to the large broad peak observed previously with the DLS analysis. It is worth noting that the poly(MMA)-latex dispersion was difficult to analyze via TEM since it was found beam-sensitive, undergoing visible disintegration and aggregation under extended time of beam exposure. In contrast, this issue did not arise with the poly(S)-latex dispersion, which remained stable and easy to analyze by TEM. Despite the presence of distinct particle sizes, it can be concluded that poly(BA-*b*-HAAC4) was successfully employed as a surfactant for the emulsion polymerization of both monomers with good results.

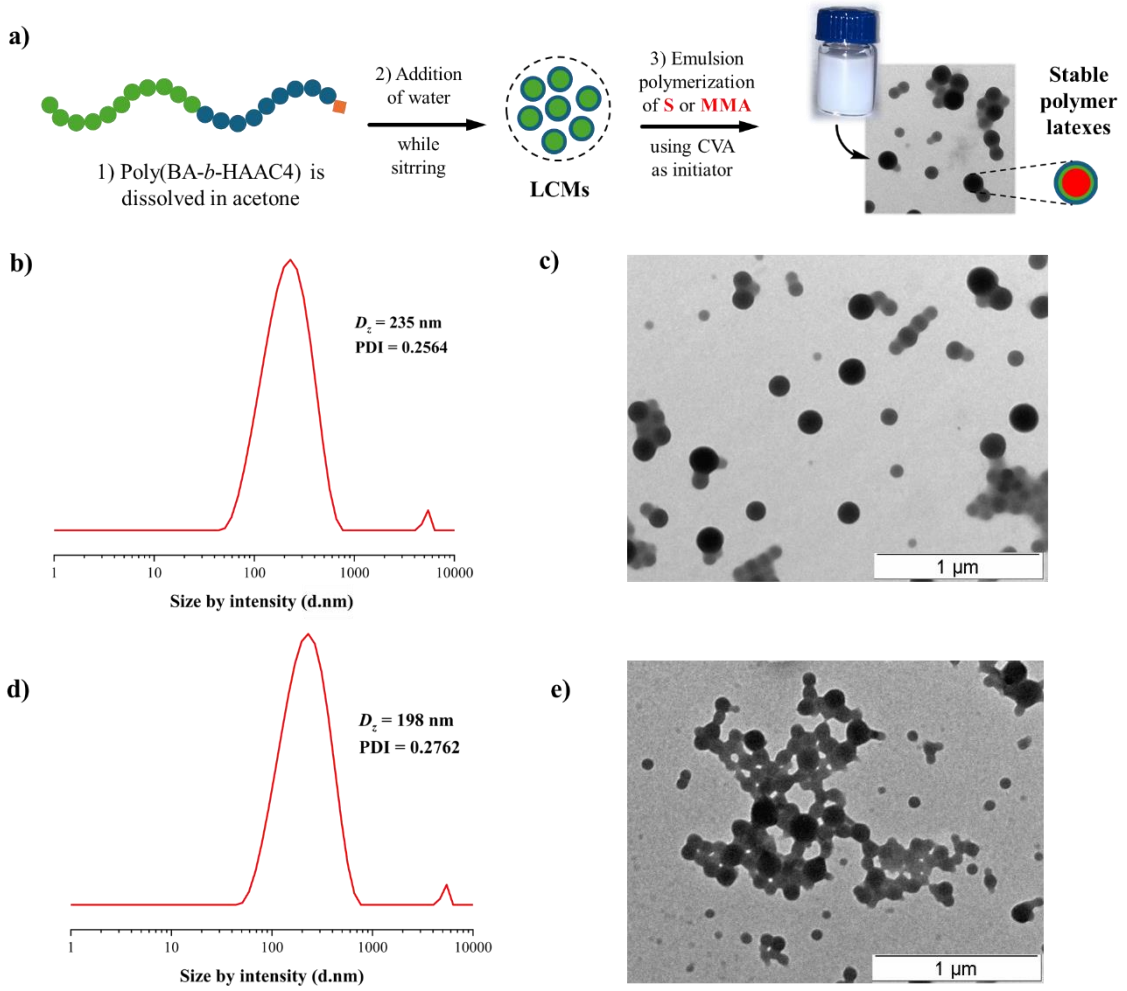

Figure 13. a) Schematic representation of the aqueous emulsion FRP of S and MMA using poly(BA-*b*-HAAC4) as stabilizer. b) DLS size distribution by intensity of poly(S)-latexes stabilized by poly(BA-*b*-HAAC4). c) TEM image of the poly(S) latex (scale bar is 100 µm). d) DLS size distribution by intensity of poly(MMA)-latexes stabilized by poly(BA-*b*-HAAC4). E) TEM image of the poly(MMA)-latex (scale bar is 100 µm).

The stability of the poly(S)-latex dispersions was assessed under various challenging conditions, as shown in Figure 14. The nonionic nature of the poly(BA-*b*-HAAC4) surfactant provided excellent pH stability to the system, since the poly(S)-latex dispersions remained stable without coagulation when the pH was increased to 14 or decreased to 1, as confirmed by DLS analysis after 24 hours. A similar stability was also observed after storing poly(S)-latex dispersion under low temperature (5 ºC) for 24 hours, depicted in Figure 14a. However, the latex dispersion broke down after being cooled -20 ºC for 24 h and subsequently thawed at room temperature, as depicted in Figure 14a. Last but not least, the poly(S)-latex dispersions showed promising stability against electrolyte addition, remaining stable even when the NaCl concentration was increased to

saturation. Both poly(S) and poly(MMA)-latex dispersions stabilized with poly(BA-*b*-HAAC4) remained stable for at least 30 days at room temperature.

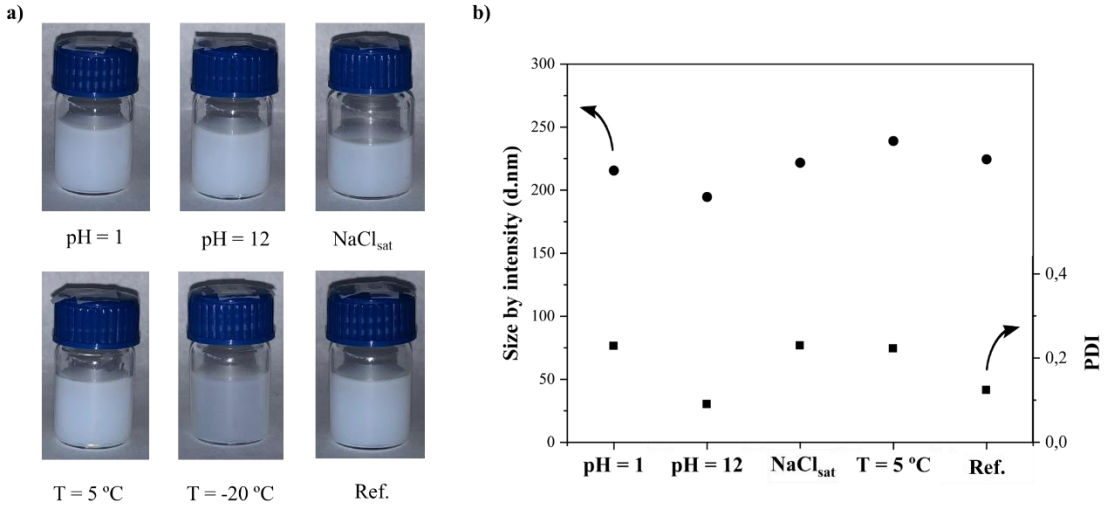

Figure 14. a) Digital images and b) DLS analysis of Poly(S)-latex dispersions under various challenging storage conditions. Ref. sample was stored at T = 25 ºC.

Thus, we can conclude that poly(BA-*b*-HAAC4) can be successfully employed as surfactant in the emulsion polymerization of both S and MMA to produce latex dispersions with high stability.

Synthesis of *N*-Ox-HAAC4 and preparation of *N*-Ox-HAAC4-HGEL for antibacterial applications

The versatility of HAAC4 also enables the easy preparation of *N*-oxide zwitterion acrylate derivatives through the oxidation of the tertiary amine. *N*-oxides have long been of considerable importance in organic and biomedical chemistry, and in recent years they have aroused increasing interest in materials and biomedical applications, due to its interesting characteristics such as antimicrobial or antifouling properties among others.[21,22]

The synthesis of *N*-oxides by oxidation of tertiary amines is straightforward and needs the use of oxidizing agents, such as H_2O_2 or a peracid such as 3-chloroperbenzoic acid (*m*CPBA). In our case, *m*CPBA was selected for carrying out the oxidation reaction, as represented in Scheme 11. 3-(4-(Acryloyoxy)butanamido)-*N*,*N*-dimethylpropan-1-amine oxide (*N*-Ox-HAAC4) was successfully obtained after 3 h of reaction at room temperature and was later purified using potassium carbonate and sodium bisulfite to eliminate 3-chlorobenzoic acid (*m*CBA) as well as rotatory evaporation to concentrate the final product. Characterization of *N*-Ox-HAAC4 is collected in Figure S16, Figure S17 and Figure S18.

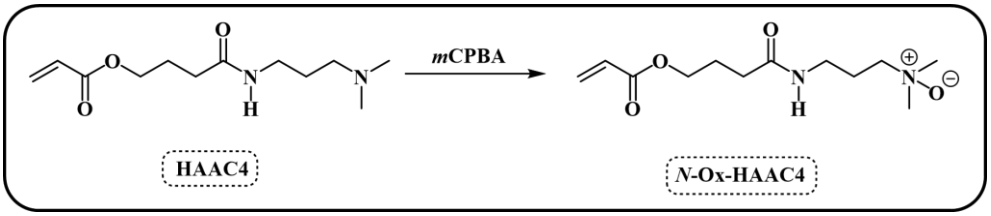

Scheme 11. Schematic representation of the synthesis of *N*-Ox-HAAC4 from HAAC4.

Owning the water-solubility of *N*-Ox-HAAC4, we envision that it could be used for the design of functional hydrogels with inherent antimicrobial properties. Accordingly, hydrogels derived from *N*-Ox-HAAC4 from now on *N*-Ox-HAAC4-HGEL were prepared using *N*-Ox-HAAC4 as monomer, *N*,*N*'-methylene bisacrylamide (MBA) as cross-linker and ammonium persulfate (APS) as the polymerization initiator in water at 65 ºC, as depicted in Figure 15a, following a stablished protocol of our laboratory.[13] Details for hydrogel preparation are found in the Experimental section. After gelation, the resulting mechanically-stable and transparent hydrogels were peeled off from the containers in the form of discs (d = 1 cm, h = 0.5 cm), and soaked and rinsed in pure water prior to further testing, as showcased in Figure 15b.

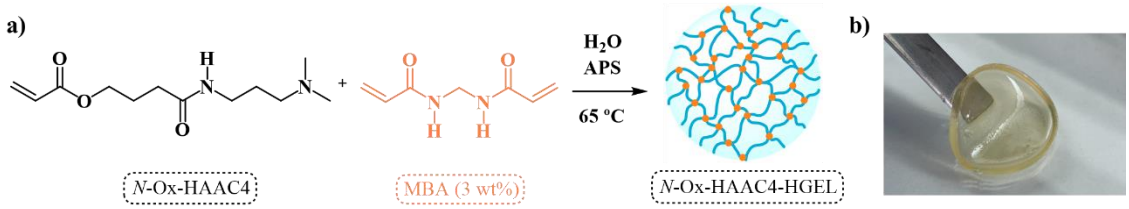

Figure 15. Preparation of hydrogels: a) Synthetic scheme for the preparation of hydrogels using MBA and APS as cross-linker and initiator, respectively. b) Digital image of *N*-Ox-HAAC4-HGEL showing the transparency and stable mechanical properties.

With the *N*-Ox-HAAC4-HGEL in our hands, its antimicrobial activity was assessed following an agar plate diffusion test (DIN EN ISO 20645:2002-02) with gram-negative *E. coli*. This method is employed to evaluate the antimicrobial properties of antimicrobial agents against specific microorganisms. In this procedure, agar plates are inoculated with a standardized inoculum of the test microorganism. Then, filter paper disc, containing the test compound at a desired concentration, or materials of interest, such as hydrogels, are placed on the agar surface. The Petri dishes are incubated under suitable conditions. Generally, antimicrobial agent diffuses into the agar and inhibits germination and growth of the test microorganism and then the diameter of inhibition growth zones is measured, indicating the effectiveness of the embedded antimicrobial agents to prevent microbial growth.[77] For comparative purpose, HAAC4-based hydrogels (HAAC4-HGEL), which do not possess any antimicrobial properties, were also synthesized

following the procedure specified in the Experimental section. Here it is worth to mention, that two cellulose discs were also used, one of them soaked in phosphate-buffered saline (PBS) solution as a negative control and another one in an ampicillin (antibiotic) solution (2 mg mL^{-1}) as a positive control. After 24 h of placing the materials on the agar plates following the spread of the *E. coli* inoculum, as can clearly be seen in Figure 16, an inhibition zone (IZ), a circular area in which the bacteria colonies do not grow, around the *N*-Ox-HAAC4-HGEL and the positive control disc were clearly visible in contrast to HAAC4-HGEL, confirming the antimicrobial properties of the *N*-Ox-HAAC4-HGEL. Table 1 collects the different IZ values obtained by this experimentation. In this case the IZ value of the HAAC4 is almost half of the IZ value of the positive control, indicating that the synthesized material is not as effective as the antibiotic in the inhibition of the *E. coli.*

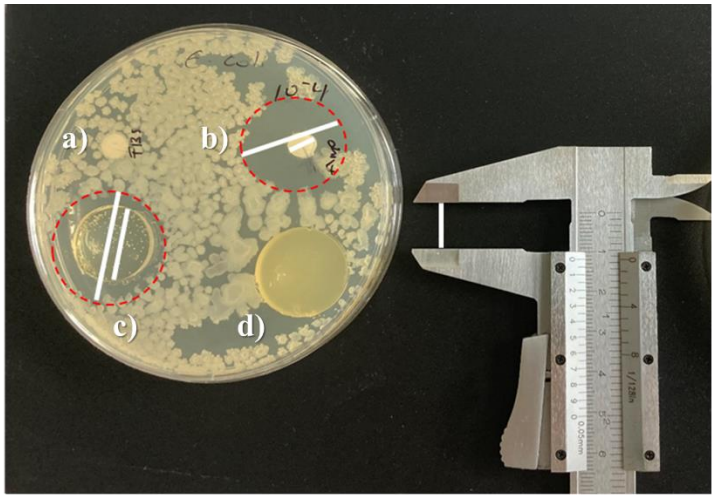

$$IZ = \frac{D - d}{2}$$

IZ: Inhibition zone
D: Diameter of sample and inhibition zone (cm)
d: Diameter of sample (cm)

Figure 16. Agar plate diffusion test (DIN EN ISO 20645:2002-02) containing a) PBS-soaked cellulose disc as negative control, b) ampicillin-soaked cellulose disc as positive control, c) *N*-Ox-HAAC4-HGEL and d) HAAC4-HGEL.

Table 1. Diameter of sample and IZ (D), diameter of sample (d), IZ values for both *N*-Ox-HAAC4-HGEL and positive control after the agar plate diffusion test (DIN EN ISO 20645:2002-02).

Material	D	d	IZ
N-Ox-HAAC4-HGEL	2.42	1.58	0.42
Positive control	2.11	0.53	0.79

Therefore, the synthesis of *N*-Ox-HAAC4-HGEL was successfully achieved. Additionally, its proven antibacterial properties could be interesting for demanding applications, such as coatings in the biomedical field, that requires the eradication of bacteria.

CONCLUSIONS

The conclusions that can be deducted from the results and analyses carried out throughout this Master's Thesis are summarized in the following points:

- The targeted 4-hydroxyamide, HAC4, was successfully synthesized in bulk conditions, and in almost quantitative yield following a catalyst-free ROA.
- CALB-mediated transesterification allowed the effective obtention of the acrylate monomer in high yield for HAAC4 using mild reaction conditions within short reaction times.
- Biphasic SET-LRP methodology was proven to be a robust method for the preparation of poly(HAAC4) at high conversion values and with near to perfect chain end fidelity.
- ABCPs based on HAAC4 and BA were successfully synthesized and characterized following a biphasic SET-LRP methodology.
- It was proven that the synthesized ABCPs poly(BA-*b*-HAAC4) can be employed as macromolecular surfactant in the aqueous emulsion polymerization of both S and MMA, leading to latexes with high stability against challenging conditions.
- The oxidation of HAAC4 with the oxidant agent *m*CPBA lead to the fruitful obtention of *N*-Ox-HAAC4.
- The antibacterial properties of the synthetized *N*-Ox-HAAC4-HGEL were evaluated and confirmed, envisioning it as a promising material for biomedical applications.

OUTLOOK

Future work should involve the study of the integration of other hydrophobic blocks from renewable sources with added functionality in the synthesis of BCPs with HAAC4. Antibacterial properties of *N*-Ox-HAAC4-HGEL against gram positive bacterial should also be studied.

Further potential applications should be investigated. LCMs should be tested for encapsulation and controlled release of hydrophobic molecules. Additionally, brush polymers containing *N*-Ox-HAAC4 as the side chain with the ultimate objective of testing their antifouling properties could also be explored. The possibility of the preparation of hydrogels derived from HAAC4 is also in the agenda, in order to access hydrogels with the ability to interact and capture CO_2.

EXPERIMENTAL SECTION

Materials

Solvents and reagents were obtained from commercial suppliers and dried and/or purified (if needed) by standard procedures. The following chemicals were purchased from Merck and used as received: acrylic acid (AA) (≥99%), 3-chloroperbenzoic acid (*m*CPBA) (<77%), 4,4'-azobis (4-cyanovaleric acid) (≥98%), ammonium persulfate (APS) (98%), butyl acrylate (BA) (≥99%), Celite® 545 AW, dimethyl sulfoxide (DMSO) (≥99%), ethyl α-bromoisobutyrate (EBiB) (98%), methyl acrylate (MA) (99%), methyl methacrylate (MMA) (99%), methyl *tert*-butyl ether (MTBE) (≥99%), *N*,*N*'-methylenebis(acrylamide) (MBA) (99%), phosphate-buffered saline (PBS) solution, tris[2-(dimethylamino)ethyl]amine (Me_6-TREN) (97%). Acetone, anhydrous magnesium sulphate (≥99%), basic aluminum oxide activated, hydrogen chloride (HCl) (37%) and dichloromethane (DCM) (≥99%) were acquired from Scharlab. Ethanol (96%) was obtained from VWR. Ampicillin sodium salt (≥91%) was purchased from Discovery Fine Chemicals. Styrene (S) (99%) was obtained from Thermo Fischer Scientific Chemicals. Dibenzylether (≥98%) was purchased from Fluka™. (Dimethylamino)-1-propylamine (DMAPA) (99%) was supplied by Hoechst Chemikalien and distilled prior use. γ-Butyrolactone (GBL) (≥99%) from Merck was dried over calcium hydride and distilled under vacuum prior use. Candida Antarctica Lipase B (CALB) inmmobilized in acrylic resin ≥5000 U/g recombinant, expressed in Aspergilius niger, acquired from Merck, was dried under vacuum over anhydrous magnesium sulphate 24 h before its use as a biocatalyst for the transesterification reactions. 4 Å molecular sieves (M-S) from Scharlab were activated 24 h at 220 ºC under vacuum. Dialysis was performed on dialysis tube cellulose benzoylated Avg, Flat width 32 mm (molecular weight cut off (MWCO) = 2000) from Merck. Deionized (DI) water was used throughout the experiments that involve particle formation. Deuterated chloroform ($CDCl_3$), deuterated dimethylsulfoxide (DMSO-d_6) and tetramethylsilane (TMS) were purchased from Eurisotop and used as received.

Methods

Nuclear magnetic resonance (NMR) spectroscopy. Proton (^{1}H NMR) and carbon (^{13}C NMR) nuclear magnetic resonance spectra were recorded on a 400 MHz (for ^{1}H) and 100.6 MHz (for ^{13}C) Varian VNMR-S400 instrument at 25 ºC in indicated deuterated solvent. All chemical shifts are quoted on the δ scale in ppm using the residual solvent as internal standard (^{1}H NMR: $CDCl_3$ = 7.26, D_2O = 4.79, $(CD_3)_2SO$ = 2.50, and ^{13}C NMR: $CDCl_3$ = 77.16, $(CD_3)SO$ = 39.52). Two-dimensional ^{13}C-^{1}H heteronuclear shift correlation spectra were recorded with the gradient heteronuclear single quantum coherence (GHSQC). ^{13}C NMR of polymer samples were recorded using a decoupling mode "nny" with a delay time (d1) = 0.5 s and a number of transients (nt) 30000. **Differential scanning calorimetry (DSC)** measurements were carried out on a Mettler

DSC3+ instrument using N_2 as a purge gas (50 mL·min^{-1}) at a heating rate of 10 ºC/min and cooling rates of 10 ºC/min in a -50 to 150 ºC temperature range for three cycles, and the second heating curve was used to determine the glass transition temperature (T_g) in the middle of the step transition. Polymer (5 to 10 mg) were encapsulated in aluminum pans before measurements. Calibration was made using an indium standard (heat flow calibration) and an indium-lead-zinc standard (temperature calibration). **Thermogravimetric analysis (TGA)** were carried out with a Mettler TGA/SDTA851e/LF/1100 with N_2 as the purge gas at a scanning rate of 10 ºC/min in a 30 to 600 ºC temperature range. **Dynamic light scattering (DLS)** measurements were carried out at room temperature using Zetasizer Ultra from Malvern Instruments equipped with a He-Ne laser. **Transmission electron microscopy (TEM)** images were recorded on a JEOL JEM-1011 TEM microscope operating with an accelerating voltage of 200 kV. Image J software was used to process the images. **LC/MS** was performed with a Thermo Scientific Vanquish Horizon UHPLC system interfaced with a Thermo scientific Orbitrap ID-X Tribrid Mass Spectrometer. Reaction's products were separated by HILIC chromatography with an ACQUITY UPLC BEH HILIC (2.1 x 150 mm, 1.7 µm) column (Waters). The mobile phase A was 50 mM ammonium acetate in water, and mobile phase B was acetonitrile. Separation was carried out under the following gradient: 0–2 min, isocratic 95% B; 2–6 min decreased to 50% B; 6–7 min, isocratic 50% B; 7-7.2 min, increased to 90% B; 7.2–10.5 min, reequilibration column 95% B. The flow was 0.4 mL min^{-1}. Samples were analyzed in fullScan mode in positive mode. The MS parameters used were scan range, 80–900 *m/z*; spray voltage, 3500 V; sheath gas, 50; auxiliary gas, 10; Ion transfer tube temperature, 300 ºC; vaporizer temperature, 300 ºC; Orbitrap resolution, 120000; RF Lens (%), 60; AGC target, 2^5; maximum injection time, 200 ms.

Experimental procedures

Synthesis of *N*-(3-(Dimethylamino)propyl)-4-hydroxybutanamide (HAC4) hydroxyamides. In a 100mL Schlenk flask under argon (Ar), previously distilled and purged with Ar GBL (5.0 g, 58.1 mmol) and DMAPA (7.0 g, 68.5 mmol) were added. The system was closed with a Teflon coated screwed cap and heated at 60 ºC. After 3h, the reaction is stopped. Traces of unreacted amine were stripped off at 60 ºC by applying vacuum under stirring overnight. Hydroxyamide HAC4 was obtained as a transparent viscous oil in 98% yield. The isolated hydroxyamide was analyzed by ^{1}H and ^{13}C NMR spectroscopy. For the kinetic experimentations periodically samples were withdrawn from the reaction solution and the consumption of the substrate and formation of HAC4 was followed via ^{1}H NMR spectroscopy.

^{1}H NMR ($CDCl_3$, TMS, δ ppm) (Figure S2): 7.29 (bs, 1H, N<u>H</u>), 4.26 (bs, 1H, O<u>H</u>), 3.60 (t, 2H, C<u>H</u>$_2$OH). 3.25 (m, 2H, CONHC<u>H</u>$_2$), 2.32–2.25 (m, 4H, C<u>H</u>$_2$CONH + C<u>H</u>$_2$N(CH$_3$)$_2$), 2.17 (s, 6H, N(C<u>H</u>$_3$)$_2$), 1.80 (m, 2H, C<u>H</u>$_2$CH$_2$OH), 1.61 (m, 2H, <u>C</u>H$_2$CH$_2$N(CH$_3$)$_2$).

^{13}C NMR (CDCl, δ ppm) (Figure S2): 173.3 (<u>C</u>ONH), 61.4 (<u>C</u>H$_2$OH), 57.5 (<u>C</u>H$_2$N(CH$_3$)$_2$), 44.7 (N(CH$_3$)$_2$), 38.5 (CONH<u>C</u>H$_2$), 33.5 (<u>C</u>H$_2$CONH), 28.2 (HOCH$_2$<u>C</u>H$_2$), 26.2 (<u>C</u>H$_2$CH$_2$N(CH$_3$)$_2$).

HRMS (LC-Orbitrap-IDX) calculated for $[M + H]^+$ $C_9H_{21}N_2O_2^+$ (m/z): 189.1603; found: 189.1608.

Synthesis of 4-((3-(Dimethylamino)propyl)amino)-4-oxobutyl acrylate (HAAC4) by CALB mediated transesterification. In a round bottom flask with a magnetic stirrer HAC4 (20.0 g, 106.2 mmol) was dissolved in MTBE (70 mL). To this mixture MA (96 mL, 1066.0 mmol) was added and immersed into an oil bath, preheated at 90 ºC. The reaction was carried out under reflux using a Soxhlet device filled with freshly activated 4Å M-S. After three cycles, CALB (1.0 g, 5 wt% with respect to HAC4) was added. After 180 min, a sample was taken for analysis of the crude product by ^{1}H NMR. Once the reaction was completed, the reaction mixture was cooled to room temperature and the enzyme was removed by filtration under Celite® 545. Then, the sample was passed through basic aluminum oxide to remove radical inhibitor. MTBE and MA were removed under vacuum, obtaining a pale-yellow viscous oil in 98% yield. The isolated monomer was analyzed by ^{1}H and ^{13}C NMR spectroscopy.

^{1}H NMR ($CDCl_3$, TMS, δ ppm) (Figure S5): 7.10 (bs, 1H, N<u>H</u>), 6.31 (dd, *J* = 17.3, 1.3 Hz, 1H, C<u>H</u>$_2$CHCOO), 6.03 (dd, *J* = 17.3, 10.5 Hz, CH$_2$C<u>H</u>COO), 5.75 (dd, *J* = 10.5, 1.3 Hz, C<u>H</u>$_2$CHCOO), 4.11 (t, 2H, COOC<u>H</u>$_2$CH$_2$), 3.22 (m, 2H, CONHC<u>H</u>$_2$), 2.27 (t, 2H, C<u>H</u>$_2$N(CH$_3$)$_2$), 2.16 (m, 2H, C<u>H</u>$_2$CONH), 2.13 (s, 6H, N(C<u>H</u>$_3$)$_2$), 1.92 (m, 2H, C<u>H</u>$_2$CH$_2$CONH), 1.56 (m, 2H, C<u>H</u>$_2$CH$_2$N(CH$_3$)$_2$).

^{13}C NMR ($CDCl_3$, δ ppm) (Figure S5): 171.5 (<u>C</u>ONH), 165.8 (CH$_2$CH<u>C</u>O), 130.4 (<u>C</u>H$_2$CHCO), 128.0 (CH$_2$<u>C</u>HCO), 63.5 (COO<u>C</u>H), 58.1 (<u>C</u>H$_2$N(CH$_3$)$_2$), 45.0 (N(<u>C</u>H$_3$)$_2$), 38.9 (CONH<u>C</u>H$_2$), 32.6 (<u>C</u>H$_2$CONH), 25.9 (<u>C</u>H$_2$CH$_2$N(CH$_3$)$_2$), 24.4 (<u>C</u>H$_2$CH$_2$CONH).

HRMS (LC-Orbitrap-IDX) calculated for $[M + H]^+$ $C_{12}H_{23}N_2O_3^+$ (m/z): 243.1709; found: 243.1714.

Synthesis of 3-(4-(Acryloyoxy)butanamido)-*N*,*N*-dimethylpropan-1-amine oxide (*N*-Ox-HAAC4). To a stirred solution of HAAC4 (3.0 g, 12.4 mmol) in DCM (3 mL) was added a solution containing 77% *m*-CPBA (3.3 g, 14.9 mmol) and DCM (40 mL) which was previously dried over $MgSO_4$. The resulting mixture was stirred at room temperature for 3 h, at which time

complete consumption of the starting material was determined by ^{1}H NMR spectroscopy. Then, the reaction mixture was diluted with DCM (15 mL), and K_2CO_3 (8.2 g, 59.4 mmol) and a small portion of sodium bisulfite were added. The resulting mixture was stirred for an additional 30 min. The solid was separated by filtration, and the filtrate was dried over $MgSO_4$ and concentrated under reduced pressure to afford the *N*-Ox-HAAC4 in yields of 90%.

^{1}H NMR ($CDCl_3$, TMS, δ ppm) (Figure S16): 8.72 (bs, 1H, NH), 6.38 (dd, *J* = 17.3, 1.5 Hz, 1H, CH_2CHCOO), 6.10 (dd, *J* = 17.3, 10.4 Hz, 1H, CH_2CHCOO), 5.80 (dd, *J* = 10.4, 1.5 Hz, 1H, CH_2CHCOO), 4.17 (t, 2H, COOCH_2CH2), 3.38 (m, 4H, CONHCH_2 + CH_2N^+–$O^-(CH_3)_2$), 3.20 (s, 6H, N^+–$O^-(CH_3)_2$), 2.28 (t, 2H, CH_2CONH), 2.10 (m, 2H, CH_2CH_2CONH), 2.01 (m, 2H, $CH_2CH_2N^+$–$O^-(CH_3)_2$).

^{13}C NMR ($CDCl_3$, δ ppm) (Figure S16): 172.8 (CONH), 166.7 (CH_2CHCO), 131.1 (CH_2CHCO), 128.9 (CH_2CHCO), 69.9 (CH_2N^+–$O^-(CH_3)_2$), 64.4 (COOCH), 59.9 (N^+–$O^-(CH_3)_2$), 38.1 (CONHCH_2), 33.3 (CH_2CONH), 25.1 ($CH_2CH_2N^+$–$O^-(CH_3)_2$), 24.0 (CH_2CH_2CONH).

HRMS (LC-Orbitrap-IDX) calculated for $[M + H]^+$ $C_{12}H_{23}N_2O_4^+$ (m/z): 259.1658; found: 259.1664.

Cu(0)-Catalyzed single electron transfer-living radical polymerization (SET-LRP) of HAAC4. The procedure is generic for the homopolymerizations conducted herein. The polymerization of HAAC4 is described with EBiB in DMSO under the following conditions: $[HAAC4]_0/[EBIB]_0/[Me_6\text{-TREN}]_0$ = 50/1/0.2 is described.

Cu(0) wire (5 cm) wrapped around a magnetic stirrer was placed in a vial with concentrated HCl (10 mL) and stirred for 30 min at room temperature. Then, the magnetic stirrer with the Cu(0) was washed with distilled water and acetone. Acetone traces were eliminated by drying under vacuum for 15 min.

A 25 mL Schlenk tube was charged with HAAC4 (0.5 g, 2.1 mmol), DMSO (0.5 mL), EBiB (6.2 µL, 41.3 µmol), Me_6-TREN (2.3 µL, 8.3 µmol) and the previously treated magnetic stirrer with the Cu(0). In the case of the homopolymerization performed with a mixture of both DMSO and H_2O (8/2, v/v), the only difference is the addition of H_2O alongside the rest of reagents. Importantly, a tiny external magnet is used to hold the stirring bar above the reaction mixture at first. By bubbling Ar through the reaction mixture for 15 min, the deoxygenation of the mixture is achieved. After that, the Schlenk tube is immersed into a water bath at 25 ºC. To start the reaction, the stirring bar with the catalyst is dropped in, defining t = 0. For the kinetic studied, a side arm of the tube was installed into the Schlenk flask and purged with Ar before removing two drops of the reaction crude using and airtight syringe under the presence of a continuous flow of

Ar. The reaction is stirred for 3h and then stopped by exposing to air the Schlenk flask. The polymer was purified by dialysis against acetone. After that, the polymer was dried in vacuo for 24 h and characterized by ^{1}H NMR and ^{13}C NMR spectroscopy. Poly(HAAC4) was obtained as yellowish viscous solid.

^{1}H NMR ($CDCl_3$, TMS, δ ppm) (Figure S8): 7.56 (bs, 1H, N<u>H</u>), 4.04 (bs, 2H, COOC<u>H</u>$_2$CH$_2$CH$_2$), 3.23 (bs, 2H, CONHC<u>H</u>$_2$), 2.36–2.15 (m, 5H, COOCH$_2$CH$_2$C<u>H</u>$_2$ + CH$_2$C<u>H</u>Br + C<u>H</u>$_2$CHBr), 2.30 (t, 2H, C<u>H</u>$_2$N(CH$_3$)$_2$), 2.22 (s, 6H, N(C<u>H</u>$_3$)$_2$), 1.90 (bs, 2H, COOCH$_2$C<u>H</u>$_2$CH$_2$), 1.64 (t, 2H, CONHCH$_2$C<u>H</u>$_2$), 1.21 (m, 3H, C<u>H</u>$_3$CHOCO), 1.09 (d, 6H, C(C<u>H</u>$_3$)$_2$).

^{13}C NMR ($CDCl_3$, δ ppm) (Figure S8): 175.4 (CH$_3$CH$_2$O<u>C</u>O), 174.6 (<u>C</u>ONH), 172.3 (<u>C</u>OOCH$_2$CH$_2$CH$_2$), 64.4 (COO<u>C</u>H$_2$CH$_2$CH2), 57.9 (<u>C</u>H$_2$N(CH$_3$)$_2$), 45.6 (N(<u>C</u>H$_3$)$_2$), 41.7 (<u>C</u>H$_2$CHBr + CH$_2$<u>C</u>HBr), 38.5 (CONH<u>C</u>H$_2$), 32.8 (<u>C</u>H$_2$CONH), 27.2 (CONHCH$_2$<u>C</u>H$_2$), 24.9 (COOCH$_2$<u>C</u>H$_2$CH$_2$).

Synthesis of poly(BA-*b*-HAAC4) block copolymer by Cu(0)-Catalyzed SET-LRP. The block copolymerization of poly(BA) ([BA]$_0$/[EBiB]$_0$/[Me$_6$-TREN]$_0$ = 50/1/0.2) with HAAC4 (50 equiv) is described.

Cu(0) wire (5 cm) wrapped around a magnetic stirrer was placed in a vial with concentrated HCl (10 mL) and stirred for 30 min at room temperature. Then, the magnetic stirrer with the Cu(0) was washed with distilled water and acetone. Acetone traces were eliminated by drying in vacuo for 15 min.

A 25 mL Schlenk tube was charged with BA (0.5 g, 3.9 mmol), DMSO (0.5 mL), EBiB (11.7 µL, 78.0 µmol) and Me$_6$-TREN (4.3 µL, 15.6 µmol) and the previously treated magnetic stirrer with the Cu(0). Importantly, a tiny external magnet is used to hold the stirring bar above the reaction mixture at first. The deoxygenation of the mixture is achieved following a Freeze-Pump-Thaw methodology. After that, the Schlenk tube is immersed into a water bath at 25 ºC. To start the reaction, the stirring bar with the catalyst is dropped in, defining t = 0. After 2 h and complete conversion of BA, a degassed solution containing HAAC4 (1.0 g, 3.9 mmol), DMSO (1.0 mL) and Me$_6$-TREN (4.3 µL, 15.6 µmol) is introduced via cannula. In the case of the copolymerization with a mixture of both DMSO and H_2O (8/2, v/v), the addition of the second monomer also includes H_2O alongside the rest of reagents. After stirring the polymerization mixture for 24 h at 25 ºC, conversion of the first and second monomers were determined by ^{1}H NMR. The copolymer was purified by dialysis against acetone. After that, the copolymer was dried in vacuo for 24 h and characterized by ^{1}H NMR and ^{13}C NMR spectroscopy. Poly(BA-*b*-HAAC4) was obtained as yellowish viscous liquid.

^{1}H NMR ($CDCl_3$, TMS, δ ppm) (Figure S12): 7.63 (bs, 1H, N<u>H</u>), 4.02 (bs, 4H, COOC<u>H</u>$_2$CH$_2$CH$_2$CH$_3$ + COOC<u>H</u>$_2$CH$_2$CH$_2$CONH), 3.22 (bs, 2H, CONHC<u>H</u>$_2$), 2.31 (t, 2H, C<u>H</u>$_2$N(CH$_3$)$_2$), 2.28–2.17 (bs, 8H, COOCH$_2$CH$_2$C<u>H</u>$_2$CONH + CH$_2$C<u>H</u>Br + C<u>H</u>$_2$CHBr + C<u>H</u>$_2$CHCH$_2$CHBr + CH$_2$C<u>H</u>CH$_2$CHBr), 2.20 (s, 6H, N(C<u>H</u>$_3$)$_2$), 1.91 (bs, 2H, COOCH$_2$C<u>H</u>$_2$CH$_2$CONH), 1.68–1.54 (bs, 4H, COOCH$_2$C<u>H</u>$_2$CH$_2$CH$_3$ + CONHCH$_2$C<u>H</u>$_2$), 1.36 (m, 2H, COOCH$_2$CH$_2$C<u>H</u>$_2$CH$_3$), 1.24 (m, 3H, C<u>H</u>$_3$CHOCO), 1.12 (d, 6H, C(C<u>H</u>$_3$)$_2$)., 0.92 (t, 3H, COOCH$_2$CH$_2$CH$_2$C<u>H</u>$_3$).

^{13}C NMR ($CDCl_3$, δ ppm) (Figure S12): 174.8–172.6 (CH2CH2O<u>C</u>O + <u>C</u>OOCH$_2$CH$_2$CH$_2$CH$_3$ + <u>C</u>OOCH$_2$CH$_2$CH$_2$CONH + <u>C</u>ONH), 64.5 (COO<u>C</u>H$_2$CH$_2$CH$_2$CH$_3$ + COO<u>C</u>H$_2$CH$_2$CH$_2$CONH), 57.6 (<u>C</u>H$_2$N(CH$_3$)$_2$), 45.5 (N(<u>C</u>H$_3$)$_2$), 41.7 (<u>C</u>HCOOCH$_2$CH$_2$CH$_2$CH$_3$ + <u>C</u>HCOOCH$_2$CH$_2$CH$_2$CONH), 38.3 (CONH<u>C</u>H$_2$), 36.3–34.5 (<u>C</u>H$_2$CHCOOCH$_2$CH$_2$CH$_2$CH$_3$ + <u>C</u>H$_2$CHCOOCH$_2$CH$_2$CH$_2$CONH), 32.7 (COOCH$_2$CH$_2$<u>C</u>H$_2$CONH), 30.7 (COOCH$_2$<u>C</u>H$_2$CH$_2$CH$_3$), 27.2 (CONHCH$_2$<u>C</u>H$_2$CH$_2$N(CH$_3$)$_2$), 24.9 (COOCH$_2$<u>C</u>H$_2$CH$_2$CONH), 19.2 (COOCH$_2$CH$_2$<u>C</u>H$_2$CH$_3$), 13.8 (COOCH$_2$CH$_2$CH$_2$<u>C</u>H$_3$).

General emulsion polymerization procedure using poly(BA-*b*-HAAC4) as stabilizer. The procedure is generic for the emulsion polymerizations conducted herein. The emulsion polymerization of S is described: 60.0 mg of the poly(BA-*b*-HAAC4) were added to a vial alongside 4.0 mg CVA and solubilized with 500.0 µL of acetone. A magnetic stirrer is added, and 4.0 mL of DI water were added while stirring, promoting the self-assembly of the copolymer. After that, the vial was sealed with a rubber septum and was deoxygenated with Ar during 15 min. Then, 0.4 g of S, which was previously passed through basic aluminum oxide, were added and the solution was stirred vigorously for 1 min. After that, the vial was placed in a thermostat bath at 65 ºC. Polymerization was allowed to proceed for 4 hours. After 4 hours, the reaction is halted, and the monomer conversion is measured using a gravimetric method. A 600.0 µL sample is taken, dried at 150 ºC, and a conversion rate of 75 % is determined. Size number and TEM analysis from latex dispersions were conducted on diluted aqueous solutions by a factor of 100.

Preparation of 4-((3-(Dimethylamino)propyl)amino)-4-oxobutyl acrylate-based hydrogel (HAAC4-HGEL). A vial containing HAAC4 (0.5 g, 2.1 mmol) and 2.5 mL of water is charged with 15.0 mg of solid MBA and stirred vigorously for 1 min. A solution containing both 12.5 mg of APS and 0.5 mL of water is prepared and added to the vial. Instantly, the mixture was transferred to various coin-like cylindrical molds under Ar flow protection. The molds were sealed and kept at 65 ºC for 24 h to allow polymerization. After that time, the hydrogels were separated carefully from the molds and rinsed with water several times.

Preparation of *N*-Ox-HAAC4-HGEL. A vial containing *N*-Ox-HAAC4 (0.45 g, 1.7 mmol), AA (0.05 g, 0.7 mmol) and 2.5 mL of water is charged with 15.0 mg of solid MBA and stirred vigorously for 1 min. A solution containing both 12.5 mg of APS and 0.5 mL of water is prepared and added to the vial. The deoxygenation of the solution is accomplished by bubbling Ar for 5 min and then the mixture was transferred to various coin-like cylindrical molds under Ar flow protection. The molds were sealed and kept at 65 ºC for 24 h to allow polymerization. After that time, the hydrogels were separated carefully from the molds and rinsed with water several times.

Antibacterial studies of *N*-Ox-HAAC4-HGEL and HAAC4-HGEL. The antibacterial activity of *N*-Ox-HAAC4-HGEL and HAAC4-HGEL were assessed against *E.coli* following DIN EN ISO 20645:2002-02 (agar-diffusion assay). *N*-Ox-HAAC4-HGEL and HAAC4-HGEL were placed, alongside a cellulose disc soaked with ampicillin (2 mg/mL) and a cellulose disc soaked in PBS solution, on a Luria–Bertani agar plate. The top layer was previously covered with 100 µL of 1.0 x 10^{-3} CFU mL^{-1} of *E. coli* (strain CECT 471) suspension. The plate was incubated for 24 h at 37 ºC. The antibacterial activity was determined as the diameters (mm) of the inhibition zone (IZ) developed surrounding the test specimen.

REFERENCES

1) Isikgor, F. H.; Becer, C. R. Lignocellulosic Biomass: A Sustainable Platform for the Production of Bio-Based Chemicals and Polymers. *Polym. Chem.* **2015**, *6*, 4497–4559.

(2) Velvizhi, G.; Goswami, C.; Shetti, N. P.; Ahmad, E.; Kishore Pant, K.; Aminabhavi, T. M. Valorisation of Lignocellulosic Biomass to Value-Added Products: Paving the Pathway towards Low-Carbon Footprint. *Fuel* **2022**, *313*, 122678.

(3) Delidovich, I.; Hausoul, P. J. C.; Deng, L.; Pfützenreuter, R.; Rose, M.; Palkovits, R. Alternative Monomers Based on Lignocellulose and Their Use for Polymer Production. *Chem. Rev.* **2016**, *116*, 1540–1599.

(4) PlasticsEurope. *Plastics-The Facts 2023*. https://plasticseurope.org/knowledge-hub/plastics-the-fast-facts-2023/ (accessed 2024-04-01).

(5) Andrady, A. L.; Neal, M. A. Applications and Societal Benefits of Plastics. *Phil. Trans. R. Soc. B* **2009**, *364*, 1977–1984.

(6) Matyjaszewski, K.; Spanswick, J. Controlled/Living Radical Polymerization. *Mater. Today* **2005**, *8*, 26–33.

(7) Corrigan, N.; Jung, K.; Moad, G.; Hawker, C. J.; Matyjaszewski, K.; Boyer, C. Reversible-Deactivation Radical Polymerization (Controlled/Living Radical Polymerization): From Discovery to Materials Design and Applications. *Prog. Polym. Sci*. **2020**, *111*, 101311.

(8) Corsaro, C.; Neri, G.; Santoro, A.; Fazio, E. Acrylate and Methacrylate Polymers' Applications: Second Life with Inexpensive and Sustainable Recycling Approaches. *Materials* **2022**, *15*, 282.

(9) Ballard, N.; Asua, J. M. Radical Polymerization of Acrylic Monomers: An Overview. *Prog. Polym. Sci*. **2018**, *79*, 40–60.

(10) Beerthuis, R.; Rothenberg, G.; Shiju, N. R. Catalytic Routes towards Acrylic Acid, Adipic Acid and ε-Caprolactam Starting from Biorenewables. *Green Chem*. **2015**, *17*, 1341–1361.

(11) Darabi Mahboub, M. J.; Dubois, J.-L.; Cavani, F.; Rostamizadeh, M.; Patience, G. S. Catalysis for the Synthesis of Methacrylic Acid and Methyl Methacrylate. *Chem. Soc. Rev.* **2018**, *47*, 7703–7738.

(12) Veith, C.; Diot-Néant, F.; Miller, S. A.; Allais, F. Synthesis and Polymerization of Bio-Based Acrylates: A Review. *Polym. Chem.* **2020**, *11*, 7452–7470.

(13) Palà, M.; El Khannaji, H.; Garay-Sarmiento, M.; Ronda, J. C.; Cádiz, V.; Galià, M.; Percec, V.; Rodriguez-Emmenegger, C.; Lligadas, G. A Green Solvent-to-Polymer Upgrading Approach to Water-Soluble LCST Poly(N-Substituted Lactamide Acrylate)s. *Green Chem.* **2022**, *24*, 8314–8323.

(14) Bensabeh, N.; Moreno, A.; Roig, A.; Rahimzadeh, M.; Rahimi, K.; Ronda, J. C.; Cádiz, V.; Galià, M.; Percec, V.; Rodriguez-Emmenegger, C.; Lligadas, G. Photoinduced Upgrading of Lactic Acid-Based Solvents to Block Copolymer Surfactants. *ACS Sustain. Chem. Eng.* **2020**, *8*, 1276–1284.

(15) Birajdar, M. S.; Joo, H.; Koh, W. G.; Park, H. Natural Bio-Based Monomers for Biomedical Applications: A Review. *Biomater. Res*. **2021**, *25*, 8.

(16) Thang, N. H.; Chien, T. B.; Cuong, D. X. Polymer-Based Hydrogels Applied in Drug Delivery: An Overview. *Gels*. **2023**, *9*, 523.

(17) Li, X.; Lan, X.; Wang, T. Highly Selective Catalytic Conversion of Furfural to γ-Butyrolactone. *Green Chem.* **2016**, *18*, 638–642.

(18) White, C.; Adam, E.; Sabri, Y.; Myers, M. B.; Pejcic, B.; Wood, C. D. Amine-Infused Hydrogels with Nonaqueous Solvents: Facile Platforms to Control CO_2 Capture Performance. *Ind. Eng. Chem. Res.* **2021**, *60*, 14758–14767.

(19) Procurement Resource. *DMAPA (Dimethylaminopropylamine) Production Cost Analysis by Chemical Reaction of Acrylonitrile and Dimethyl Amine*. https://www.procurementresource.com/cost-analysis/dmapa-production-by-chemical-reaction-of-acrylonitrile-and-dimethyl-amine (accessed 2024-06-06).

(20) Mack, D.; Schätzle, S.; Traa, Y.; Klemm, E. Synthesis of Acrylonitrile from Renewable Lactic Acid. *ChemSusChem* **2019**, *12*, 1653–1663.

(21) Burmeister, N.; Zorn, E.; Farooq, A.; Preuss, L.; Vollstedt, C.; Friedrich, T.; Mantel, T.; Scharnagl, N.; Rohnke, M.; Ernst, M.; Wicha, S. G.; Streit, W. R.; Maison, W. Surface Grafted *N*-Oxides Have Low-Fouling and Antibacterial Properties. *Adv. Mater. Interfaces* **2023**, *10*, 2300505.

(22) Kobus, M.; Friedrich, T.; Zorn, E.; Burmeister, N.; Maison, W. Medicinal Chemistry of Drugs with *N*-Oxide Functionalities. *J. Med. Chem*. **2024**, *67*, 5168–5184.

(23) Bensabeh, N.; Moreno, A.; Roig, A.; Monaghan, O. R.; Ronda, J. C.; Cádiz, V.; Galià, M.; Howdle, S. M.; Lligadas, G.; Percec, V. Polyacrylates Derived from Biobased Ethyl Lactate Solvent via SET-LRP. *Biomacromolecules* **2019**, *20*, 2135–2147.

(24) Diot-Néant, F.; Rastoder, E.; Miller, S. A.; Allais, F. Chemo-Enzymatic Synthesis and Free Radical Polymerization of Renewable Acrylate Monomers from Cellulose-Based Lactones. *ACS Sustain. Chem. Eng.* **2018**, *6*, 17284–17293.

(25) Banik, S. D.; Nordblad, M.; Woodley, J. M.; Peters, G. H. Effect of Water Clustering on the Activity of Candida antarctica Lipase B in Organic Medium. *Catalysts* **2017**, *7*, 227.

(26) Percec, V.; Popov, A. V.; Ramirez-Castillo, E.; Monteiro, M.; Barboiu, B.; Weichold, O.; Asandei, A. D.; Mitchell, C. M. Aqueous Room Temperature Metal-Catalyzed Living Radical Polymerization of Vinyl Chloride. *J. Am. Chem. Soc.* **2002**, *124*, 4940–4941.

(27) Lligadas, G.; Grama, S.; Percec, V. Single-Electron Transfer Living Radical Polymerization Platform to Practice, Develop, and Invent. *Biomacromolecules* **2017**, *18*, 2981–3008.

(28) Anastasaki, A.; Nikolaou, V.; Nurumbetov, G.; Wilson, P.; Kempe, K.; Quinn, J. F.; Davis, T. P.; Whittaker, M. R.; Haddleton, D. M. Cu(0)-Mediated Living Radical Polymerization: A Versatile Tool for Materials Synthesis. *Chem. Rev*. **2016**, *116*, 835–877.

(29) Percec, V.; Guliashvili, T.; Ladislaw, J. S.; Wistrand, A.; Stjerndahl, A.; Sienkowska, M. J.; Monteiro, M. J.; Sahoo, S. Ultrafast Synthesis of Ultrahigh Molar Mass Polymers by Metal-Catalyzed Living Radical

Polymerization of Acrylates, Methacrylates, and Vinyl Chloride Mediated by SET at 25 °C. *J. Am. Chem. Soc.* **2006**, *128*, 14156–14165.

(30) Rosen, B. M.; Percec, V. Single-Electron Transfer and Single-Electron Transfer Degenerative Chain Transfer Living Radical Polymerization. *Chem. Rev.* **2009**, *109*, 5069–5119.

(31) Guliashvili, T.; Percec, V. A Comparative Computational Study of the Homolytic and Heterolytic Bond Dissociation Energies Involved in the Activation Step of ATRP and SET-LRP of Vinyl Monomers. *J. Polym. Sci., Part A: Polym. Chem.* **2007**, *45*, 1607–1618.

(32) Ching, Y. L.; Coote, M. L.; Gennaro, A.; Matyjaszewski, K. Ab Initio Evaluation of the Thermodynamic and Electrochemical Properties of Alkyl Halides and Radicals and Their Mechanistic Implications for Atom Transfer Radical Polymerization. *J. Am. Chem. Soc.* **2008**, *130*, 12762–12774.

(33) Isse, A. A.; Gennaro, A.; Lin, C. Y.; Hodgson, J. L.; Coote, M. L.; Guliashvili, T. Mechanism of Carbon-Halogen Bond Reductive Cleavage in Activated Alkyl Halide Initiators Relevant to Living Radical Polymerization: Theoretical and Experimental Study. *J. Am. Chem. Soc.* **2011**, *133*, 6254–6264.

(34) Moreno, A. Cu(0) Wire-Mediated SET-LRP in Biphasic Systems and Development of Stimuli Cleavable Polymers. Ph.D. Thesis, Universitat Rovira i Virgili, Tarragona, Spain, **2018**.

(35) Lligadas, G.; Rosen, B. M.; Bell, C. A.; Monteiro, M. J.; Percec, V. Effect of Cu(0) Particle Size on the Kinetics of SET-LRP in DMSO and Cu-Mediated Radical Polymerization in MeCN at 25 °C. *Macromolecules* **2008**, *41*, 8365–8371.

(36) Lligadas, G.; Percec, V. Ultrafast SET-LRP of Methyl Acrylate at 25 °C in Alcohols. *J. Polym. Sci., Part A: Polym. Chem.* **2008**, *46*, 2745–2754.

(37) Rosen, B. M.; Percec, V. Implications of Monomer and Initiator Structure on the Dissociative Electron-Transfer Step of SET-LRP. *J. Polym. Sci., Part A: Polym. Chem.* **2008**, *46*, 5663–5697.

(38) Nguyen, N. H.; Levere, M. E.; Percec, V. TREN versus Me_6-TREN as Ligands in SET-LRP of Methyl Acrylate. *J. Polym. Sci., Part A: Polym. Chem.* **2012**, *50*, 35–46.

(39) Rosen, B. M.; Percec, V. A Density Functional Theory Computational Study of the Role of Ligand on the Stability of Cu^{I} and Cu^{II} Species Associated with ATRP and SET-LRP. *J. Polym. Sci., Part A: Polym. Chem.* **2007**, *45*, 4950–4964.

(40) Bensabeh, N.; Moreno, A.; Maurya, D. S.; Adamson, J.; Galià, M.; Lligadas, G.; Percec, V. Resolving the Incompatibility between SET-LRP and Non-Disproportionating Solvents. *Giant* **2023**, *15*, 100176.

(41) Rosen, B. M.; Jiang, X.; Wilson, C. J.; Nguyen, N. H.; Monteiro, M. J.; Percec, V. The Disproportionation of Cu(I)X Mediated by Ligand and Solvent into Cu(0) and Cu(II)X_2 and Its Implications for SET-LRP. *J. Polym. Sci., Part A: Polym. Chem.* **2009**, *47*, 5606–5628.

(42) Wang, C.; Wang, Z.; Zhang, X. Amphiphilic Building Blocks for Self-Assembly: From Amphiphiles to Supra-Amphiphiles. *Acc. Chem. Res.* **2012**, *45*, 608–618.

(43) Lombardo, D.; Kiselev, M. A.; Magazù, S.; Calandra, P. Amphiphiles Self-Assembly: Basic Concepts and Future Perspectives of Supramolecular Approaches. *Adv. Condens. Matter Phys*. **2015**, *1*, 151683.

(44) Mai, Y.; Eisenberg, A. Self-Assembly of Block Copolymers. *Chem. Soc. Rev.* **2012**, *41*, 5969–5985.

(45) Adams, M. L.; Lavasanifar, A.; Kwon, G. S. Amphiphilic block copolymers for drug delivery. *J. Pharm. Sci.* **2003**, *92*, 1343–1355.

(46) Epps, T. H.; O'Reilly, R. K. Block Copolymers: Controlling Nanostructure to Generate Functional Materials - Synthesis, Characterization, and Engineering. *Chem. Sci.* **2016**, *7*, 1674–1689.

(47) Kuperkar, K.; Patel, D.; Atanase, L. I.; Bahadur, P. Amphiphilic Block Copolymers: Their Structures, and Self-Assembly to Polymeric Micelles and Polymersomes as Drug Delivery Vehicles. *Polymers* **2022**, *14*, 4702.

(48) Riess, G.; Labbe, C. Block Copolymers in Emulsion and Dispersion Polymerization. *Macromol. Rapid Commun*. **2004**, 25, 401–435.

(49) Muñoz-Bonilla, A.; Ali, S. I.; Del Campo, A.; Fernández-García, M.; Van Herk, A. M.; Heuts, J. P. A. Block Copolymer Surfactants in Emulsion Polymerization: Influence of the Miscibility of the Hydrophobic Block on Kinetics, Particle Morphology, and Film Formation. *Macromolecules* **2011**, *44*, 4282–4290.

(50) Mehta, P.; Sharma, M.; Devi, M. Hydrogels: An Overview of Its Classifications, Properties, and Applications. *J. Mech. Behav. Biomed. Mater*. **2023**, *147*, 106145.

(51) Correa, S.; Grosskopf, A. K.; Lopez Hernandez, H.; Chan, D.; Yu, A. C.; Stapleton, L. M.; Appel, E. A. Translational Applications of Hydrogels. *Chem. Rev*. **2021**, *121*,11385–11457.

(52) Khan, F.; Atif, M.; Haseen, M.; Kamal, S.; Khan, M. S.; Shahid, S.; Nami, S. A. A. Synthesis, Classification and Properties of Hydrogels: Their Applications in Drug Delivery and Agriculture. *J. Mater. Chem. B* **2022**, *10*, 170–203.

(53) Ho, T. C.; Chang, C. C.; Chan, H. P.; Chung, T. W.; Shu, C. W.; Chuang, K. P.; Duh, T. H.; Yang, M. H.; Tyan, Y. C. Hydrogels: Properties and Applications in Biomedicine. *Molecules* **2022**, *27*, 2902.

(54) Zhang, Z.; Fu, H.; Li, Z.; Huang, J.; Xu, Z.; Lai, Y.; Qian, X.; Zhang, S. Hydrogel Materials for Sustainable Water Resources Harvesting & Treatment: Synthesis, Mechanism and Applications. *Chem. Eng. J*. **2022**, *439*, 135756.

(55) Gao, Y.; Peng, K.; Mitragotri, S. Covalently Crosslinked Hydrogels via Step-Growth Reactions: Crosslinking Chemistries, Polymers, and Clinical Impact. *Adv. Mater*. **2021**, *33*, 2006362.

(56) Lin, S.; Liu, X.; Liu, J.; Yuk, H.; Loh, H.-C.; Parada, G. A.; Settens, C.; Song, J.; Masic, A.; Mckinley, G. H.; Zhao, X. Anti-Fatigue-Fracture Hydrogels. *Sci. Adv.* **2019**, *5*, eaau8528.

(57) Zhang, Y. S.; Khademhosseini, A. Advances in Engineering Hydrogels. *Science* **2017**, *356*, eaaf3627.

(58) Sun, W.; Xue, B.; Li, Y.; Qin, M.; Wu, J.; Lu, K.; Wu, J.; Cao, Y.; Jiang, Q.; Wang, W. Polymer-Supramolecular Polymer Double-Network Hydrogel. *Adv. Funct. Mater.* **2016**, *26*, 9044–9052.

(59) Liu, X.; He, X.; Yang, B.; Lai, L.; Chen, N.; Hu, J.; Lu, Q. Dual Physically Cross-Linked Hydrogels Incorporating Hydrophobic Interactions with Promising Repairability and Ultrahigh Elongation. *Adv. Funct. Mater.* **2021**, *31*, 2008187.

(60) Pranantyo, D.; Yeo, C. K.; Wu, Y.; Fan, C.; Xu, X.; Yip, Y. S.; Vos, M. I. G.; Mahadevegowda, S. H.; Lim, P. L. K.; Yang, L.; Hammond, P. T.; Leavesley, D. I.; Tan, N. S.; Chan-Park, M. B. Hydrogel Dressings with Intrinsic Antibiofilm and Antioxidative Dual Functionalities Accelerate Infected Diabetic Wound Healing. *Nat. Commun.* **2024**, *15*, 954.

(61) Guo, Z.; Dong, L.; Xia, J.; Mi, S.; Sun, W. 3D Printing Unique Nanoclay-Incorporated Double-Network Hydrogels for Construction of Complex Tissue Engineering Scaffolds. *Adv. Healthc. Mater.* **2021**, *10*, 2100036.

(62) Alemán, C.; Betran, O.; Casanovas, J.; Houk, K. N.; Hall, H. K. Thermodynamic Control of the Polymerizability of Five-, Six-, and Seven-Membered Lactones. *J. Org. Chem.* **2009**, *74*, 6237–6244.

(63) Gustafsson, T.; Pontén, F.; Seeberger, P. H. Trimethylaluminium Mediated Amide Bond Formation in a Continuous Flow Microreactor as Key to the Synthesis of Rimonabant and Efaproxiral. *Chem. Commun.* **2008**, *9*, 1100–1102.

(64) Lalli, C.; Trabocchi, A.; Menchi, G.; Guarna, A. $LiNTf_2$-Catalyzed Aminolysis of Lactones with Stoichiometric Quantities of Amines. *Synlett* **2008**, *2*, 189–192.

(65) Guo, W.; Gómez, J. E.; Martínez-Rodríguez, L.; Bandeira, N. A. G.; Bo, C.; Kleij, A. W. Metal-Free Synthesis of N-Aryl Amides Using Organocatalytic Ring-Opening Aminolysis of Lactones. *ChemSusChem* **2017**, *10*, 1969–1975.

(66) Popescu, D.; Hoogenboom, R.; Keul, H.; Moeller, M. Hydroxy Functional Acrylate and Methacrylate Monomers Prepared via Lipase-Catalyzed Transacylation Reactions. *J. Mol. Catal. B Enzym.* **2010**, *62*, 80–89.

(67) Nguyen, N. H.; Percec, V. Disproportionating versus Nondisproportionating Solvent Effect in the SET-LRP of Methyl Acrylate during Catalysis with Nonactivated and Activated Cu(0) Wire. *J. Polym. Sci., Part A: Polym. Chem.* **2011**, *49* (19), 4227–4240.

(68) Moreno, A.; Grama, S.; Liu, T.; Galià, M.; Lligadas, G.; Percec, V. SET-LRP Mediated by TREN in Biphasic Water-Organic Solvent Mixtures Provides the Most Economical and Efficient Process. *Polym. Chem.* **2017**, *8*, 7559–7574.

(69) Shahrbabaki, Z.; Oveissi, F.; Farajikhah, S.; Ghasemian, M. B.; Jansen-Van Vuuren, R. D.; Jessop, P. G.; Yun, J.; Dehghani, F.; Naficy, S. Electrical Response of Poly(N-[3-(Dimethylamino)Propyl] Methacrylamide) to CO_2 at a Long Exposure Period. *ACS Omega* **2022**, *7*, 22232–22243.

(70) The Insight Partners. *Butyl Acrylate Market Size, Share and Industry Trends -2028.* https://www.theinsightpartners.com/reports/butyl-acrylate-market/ (accessed 2024-07-01).

(71) Constantino, D. S. M.; Faria, R. P. V; Ribeiro, A. M.; Rodrigues, Alírio. E. Butyl Acrylate Production: A Review on Process Intensification Strategies. *Chem. Eng. Process.* **2019**, *142*, 107563.

(72) Niesbach, A.; Lutze, P.; Górak, A. Reactive Distillation for Production of N-Butyl Acrylate from Bio-Based Raw Materials. In *Comput. Aided Chem. Eng.* **2013**, *32*, 223–228.

(73) Ewing, T. A.; Nouse, N.; van Lint, M.; van Haveren, J.; Hugenholtz, J.; van Es, D. S. Fermentation for the Production of Biobased Chemicals in a Circular Economy: A Perspective for the Period 2022-2050. *Green Chem.* **2022**, *24*, 6373–6405.

(74) Asua, J. M. Emulsion Polymerization: From Fundamental Mechanisms to Process Developments. *J. Polym. Sci., Part A: Polym. Chem*. **2004**, *42*, 1025–1041.

(75) Raffa, P.; Wever, D. A. Z.; Picchioni, F.; Broekhuis, A. A. Polymeric Surfactants: Synthesis, Properties, and Links to Applications. *Chem. Rev*. **2015**, *115*, 8504–8563.

(76) George, S. R.; Champagne-Hartley, R.; Deeter, G. A.; Campbell, J. D.; Reck, B.; Urban, D.; Cunningham, M. F. Amphiphilic Block Copolymers as Stabilizers in Emulsion Polymerization: Effects of the Anchoring Block Molecular Weigh Dispersity on Stabilization Performance. *Macromolecules* **2017**, *50*, 315–323.

(77) Balouiri, M.; Sadiki, M.; Ibnsouda, S. K. Methods for in Vitro Evaluating Antimicrobial Activity: A Review. *J. Pharm. Anal*. **2016**, *6*, 71–79.

Alba Tirado Bermúdez

SUPPLEMENTARY INFORMATION of

Valorization of Forestry Derivatives into Functional Acrylic Polymers for Specific Applications

MASTER'S THESIS

Supervised by Dr. Adrian Moreno Guerra and Prof. Juan Carlos Ronda Bargalló

Master in Synthesis, Catalysis and Molecular Design

Analytical Chemistry and Organic Chemistry Department

UNIVERSITAT ROVIRA i VIRGILI

Tarragona

2023–2024

TABLE OF CONTENTS

Kinetic experimentation of ROA of GBL and DMAPA for the obtention of HAC4 precursor

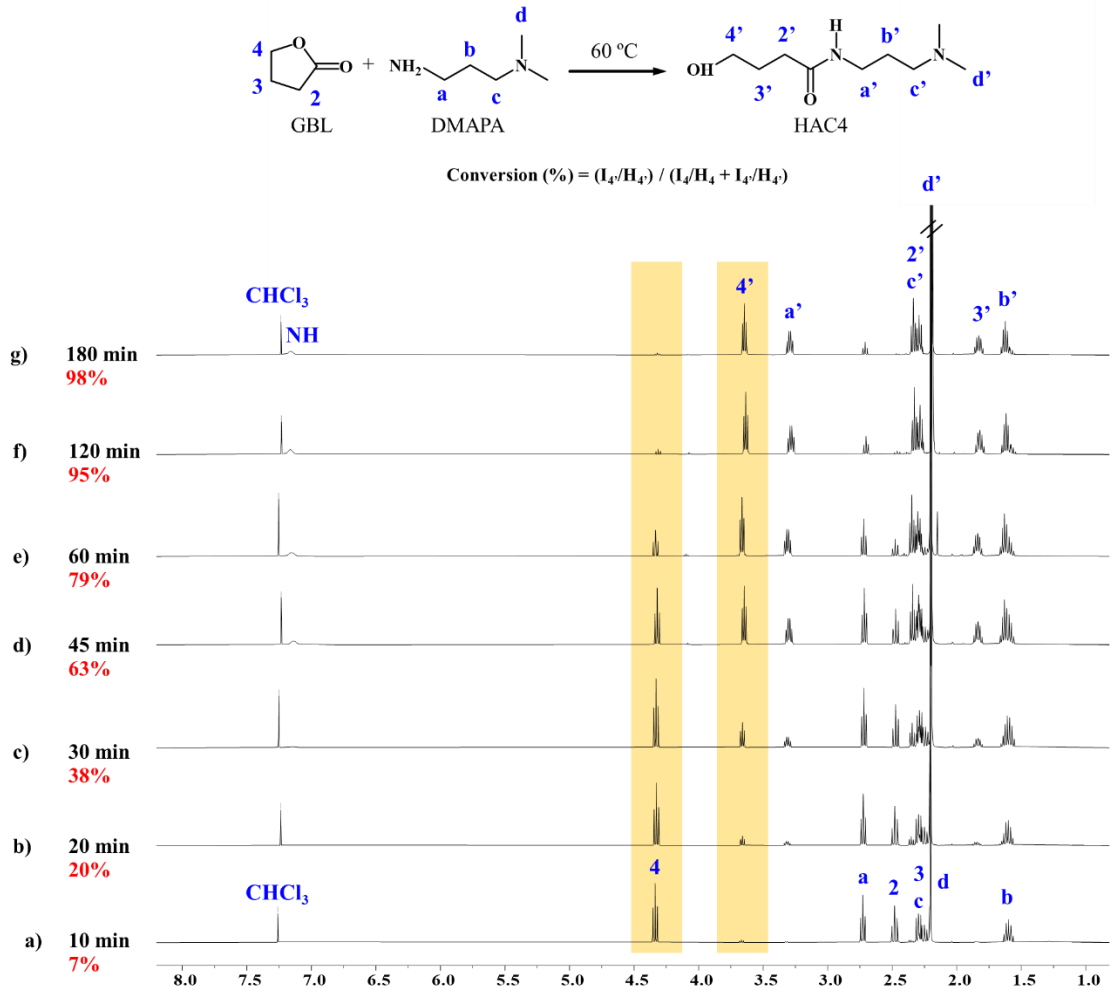

Figure S1. Superposed ^{1}H NMR spectra of GBL and DMAPA and the mixture of reaction after a) 10 min; b) 20 min; c) 30 min; d) 45 min; e) 60 min; f) 120 min and e) 180 min at 60 ºC. The assignments of the different signals are shown.

Structural Characterization of HAC4

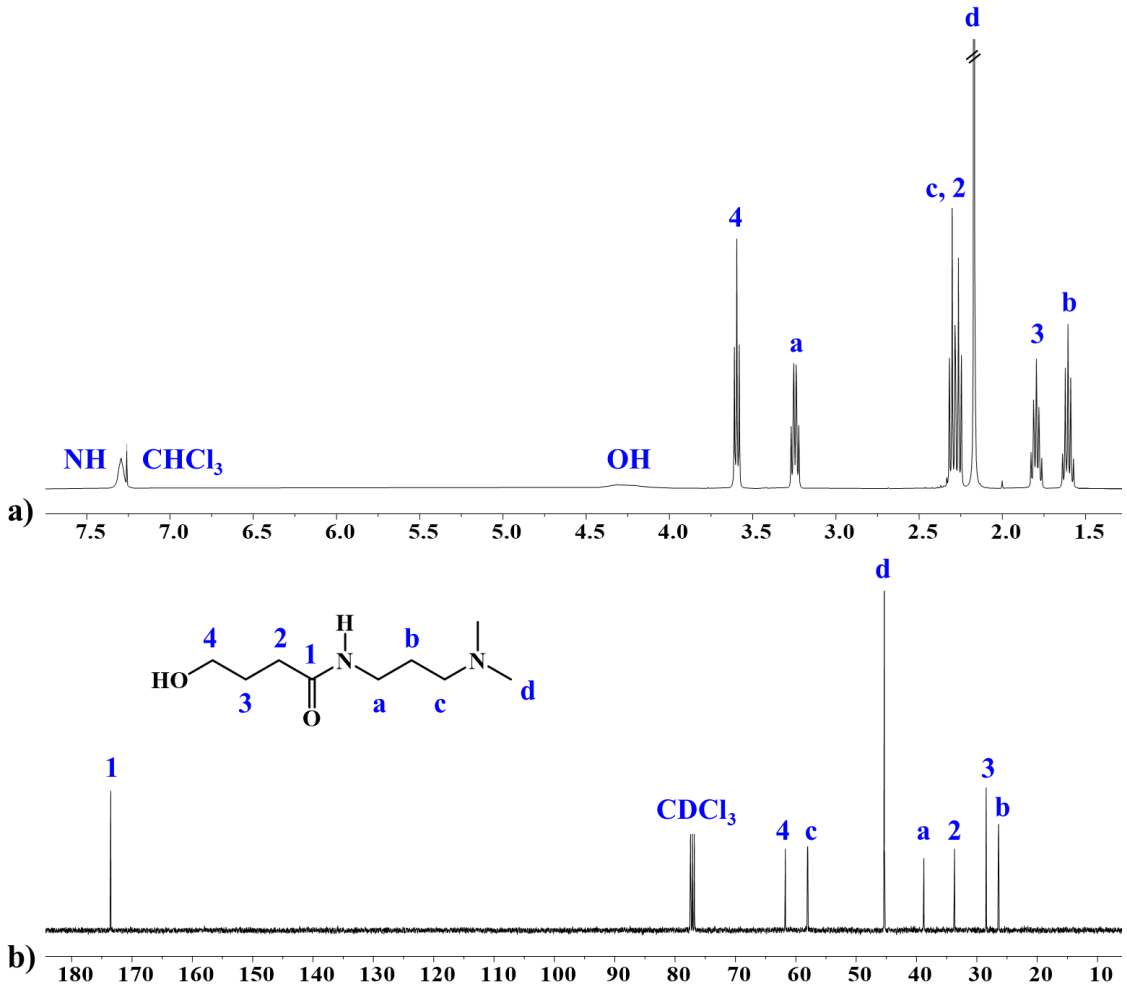

Figure S2. a) ^{1}H and b) ^{13}C NMR spectra of HAC4 recorded in $CDCl_3$.

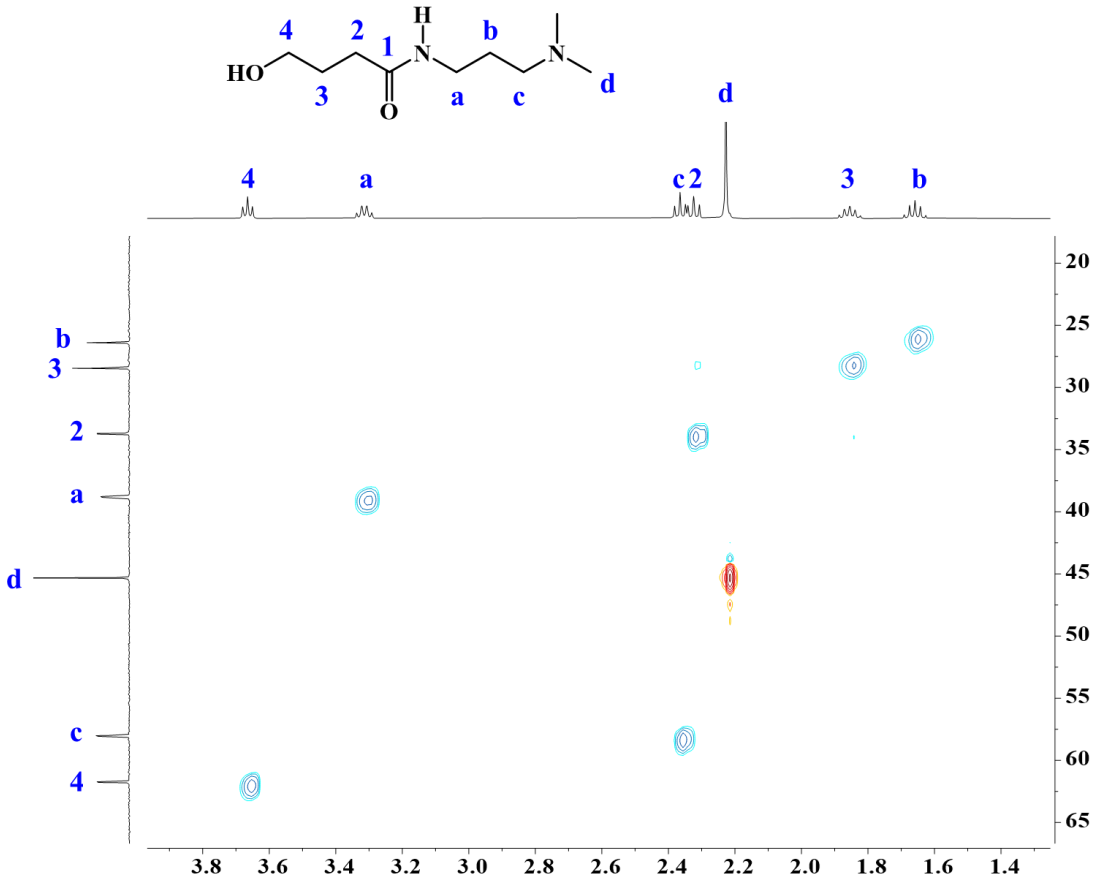

Figure S3. GHSQC correlation spectrum of HAC4 recorded in $CDCl_3$.

Kinetic experimentation of CALB-mediated transesterification of HAC4 for the obtention of HAAC4 monomer

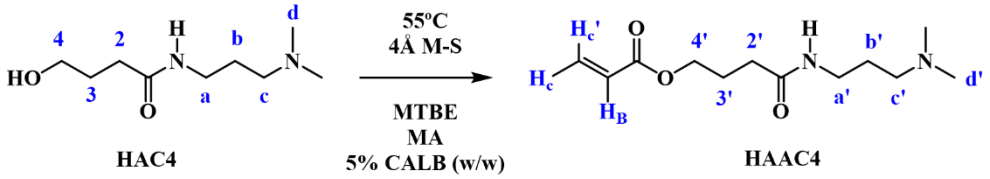

Conversion (%) = $(I_{4'}/H_{4'}) / (I_4/H_4 + I_{4'}/H_{4'})$

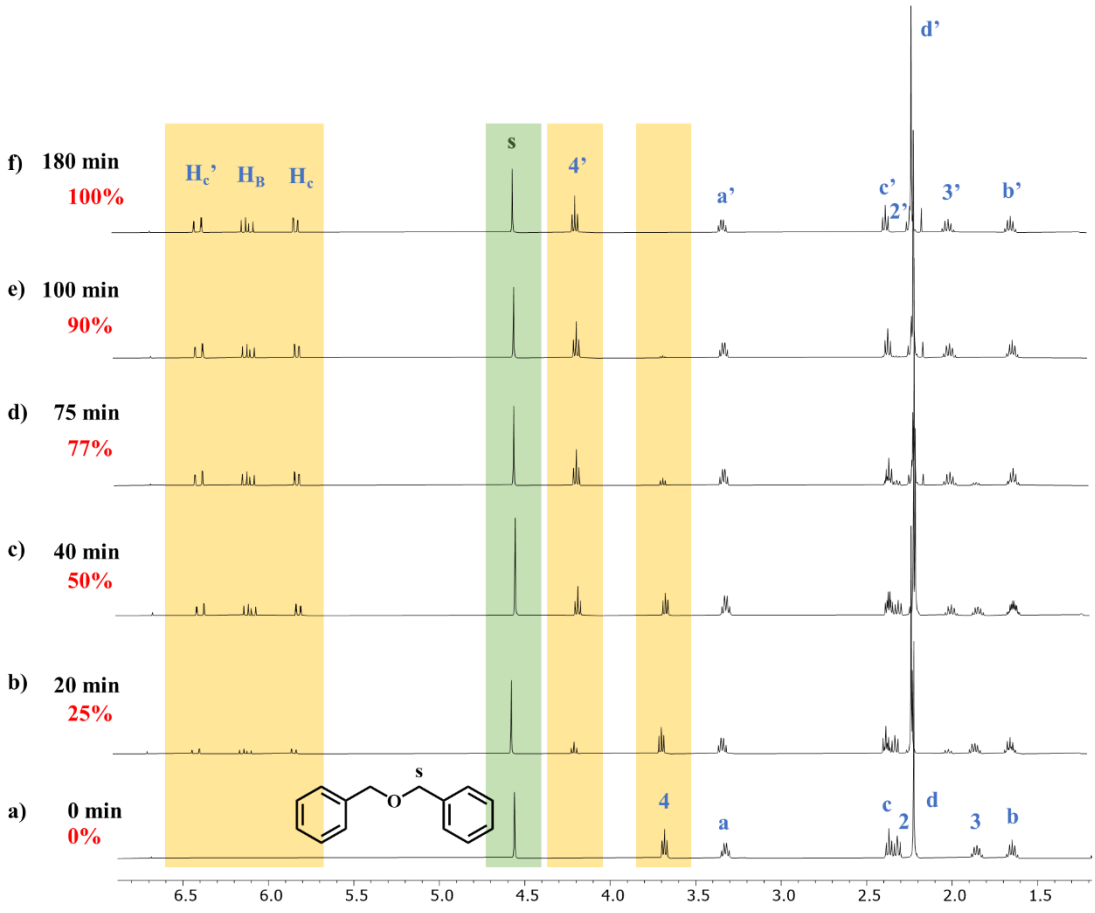

Figure S4. Superposed ^{1}H NMR spectra of HAC4 and the mixture of reaction after a) 0 min; b) 20 min; c) 40 min; d) 75 min; e) 100 min and f) 180 min in the reaction with MA catalyzed with CALB in MTBE at 90 ºC. The assignments of the different signals are shown. Reaction conditions: [HAC4] = 0.07 M; [dibenzylether] = 0.03 M.

Structural Characterization of HAAC4

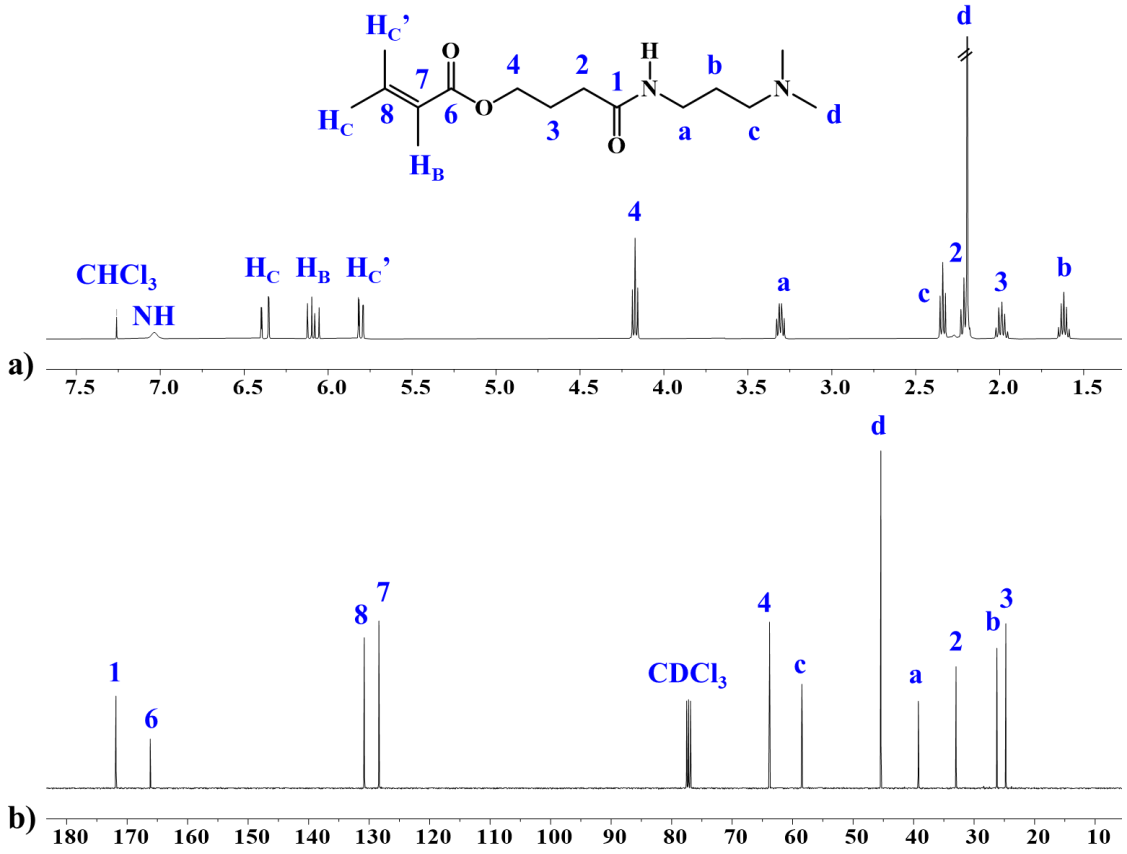

Figure S5. a) ^{1}H and b) ^{13}C NMR spectra of HAAC4 recorded in $CDCl_3$.

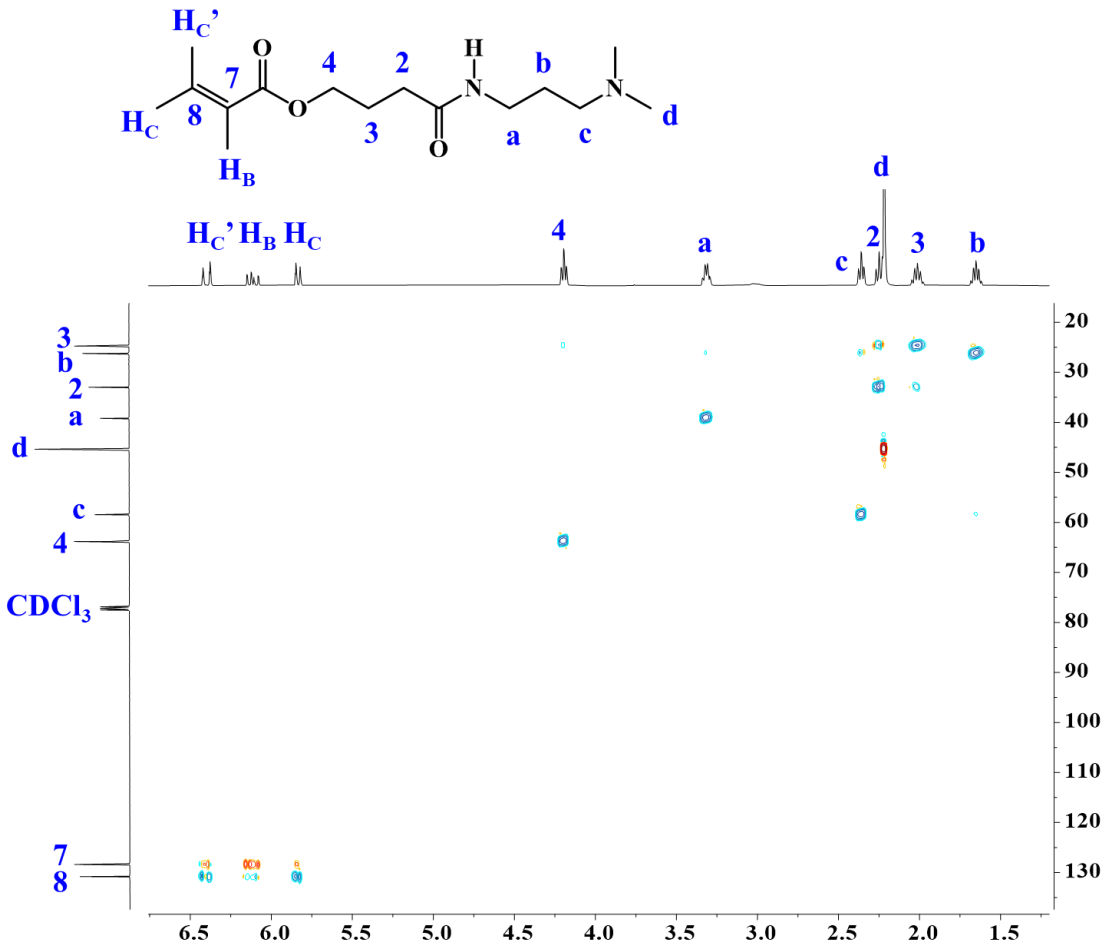

Figure S6. GHSQC correlation spectrum of HAAC4 recorded in $CDCl_3$.

Kinetic experimentation of HAAC4 SET-LRP homopolymerization for the obtention of poly(HAAC4)

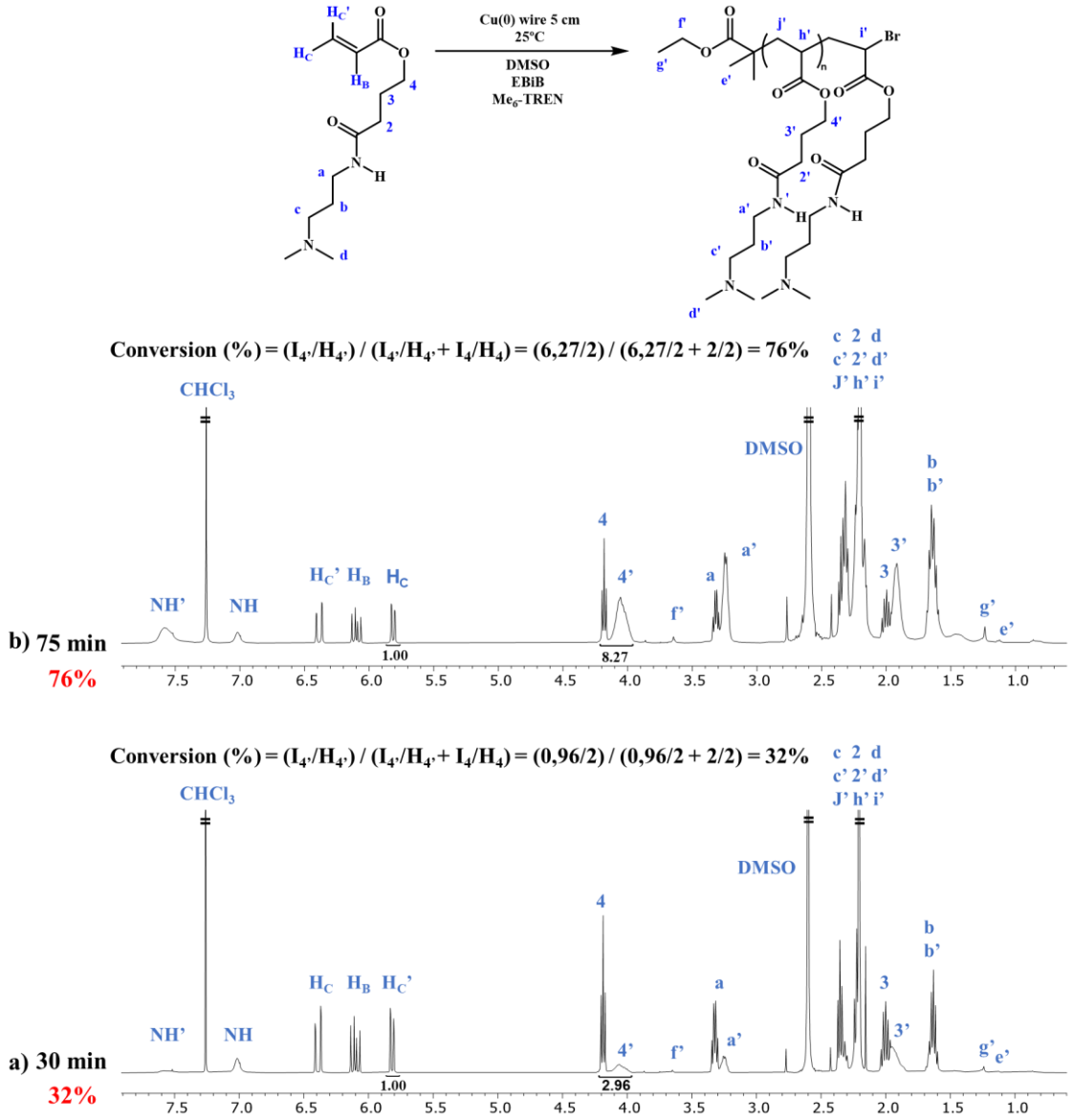

Figure S7. Superposed ^{1}H NMR spectra of HAAC4 and the reaction mixture after a) 30 min and b) 75 min in the SET-LRP reaction.

Structural Characterization of Poly(HAAC4) synthesized by SET-LRP

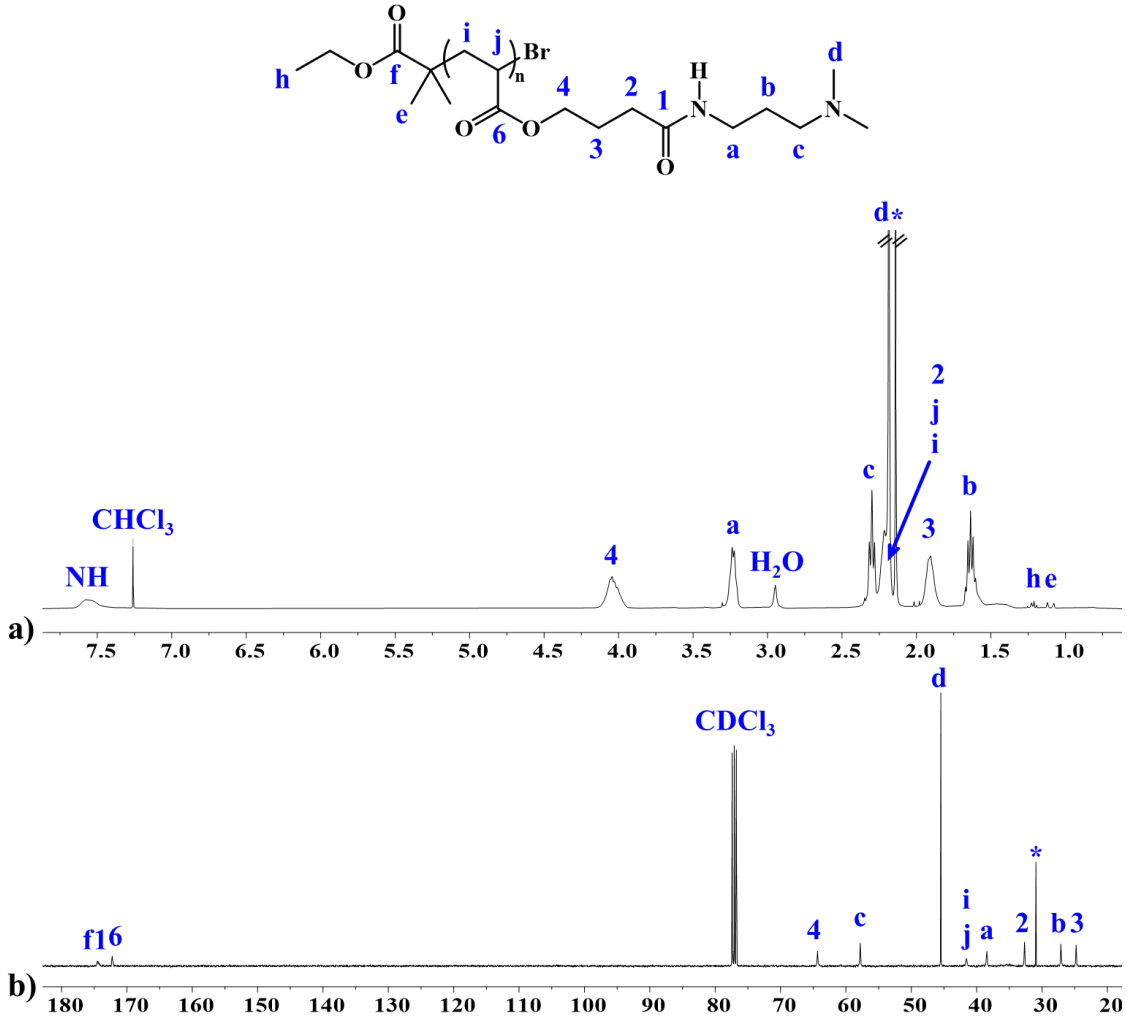

*acetone traces

Figure S8. a) ^{1}H and b) ^{13}C NMR spectra of poly(HAAC4) recorded in $CDCl_3$.

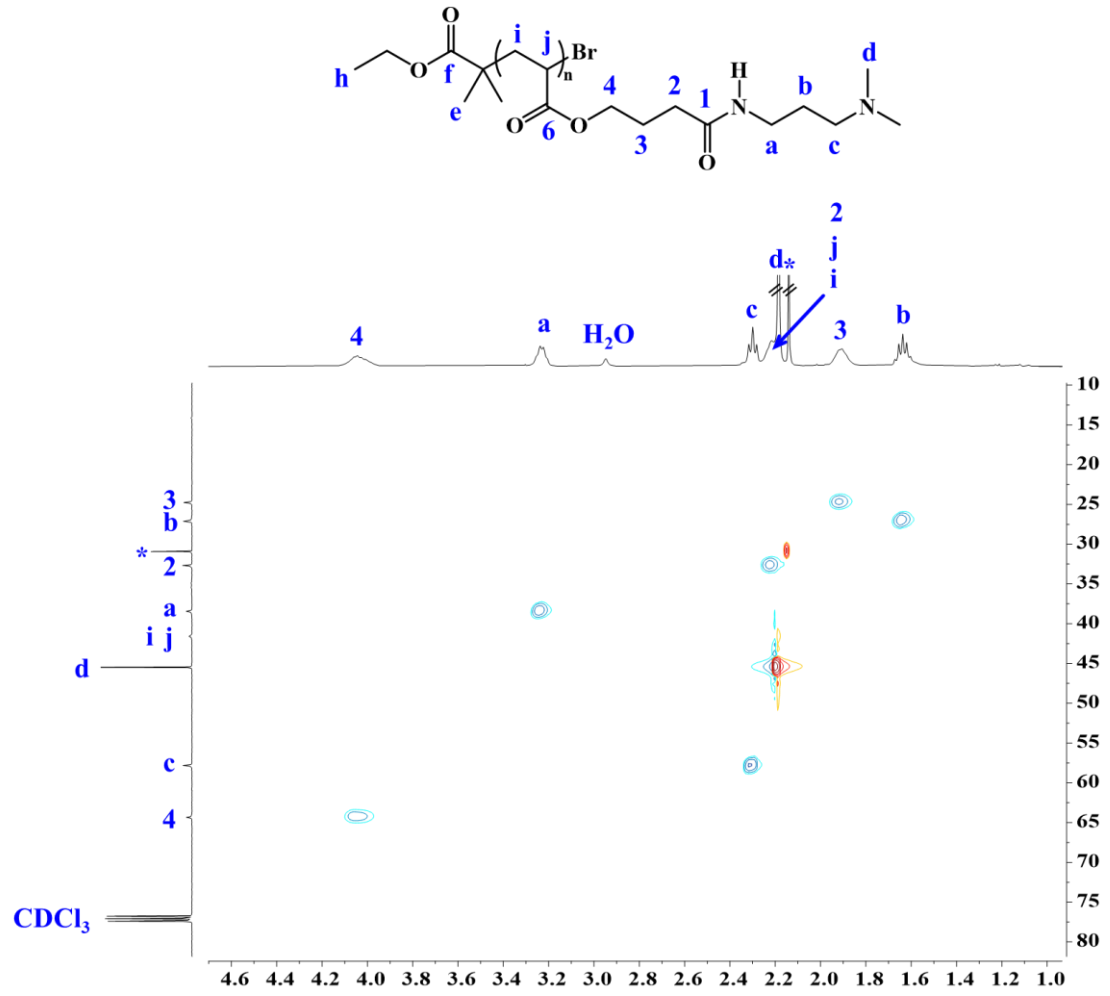

*acetone traces

Figure S9. GHSQC correlation spectrum of poly(HAAC4) recorded in $CDCl_3$.

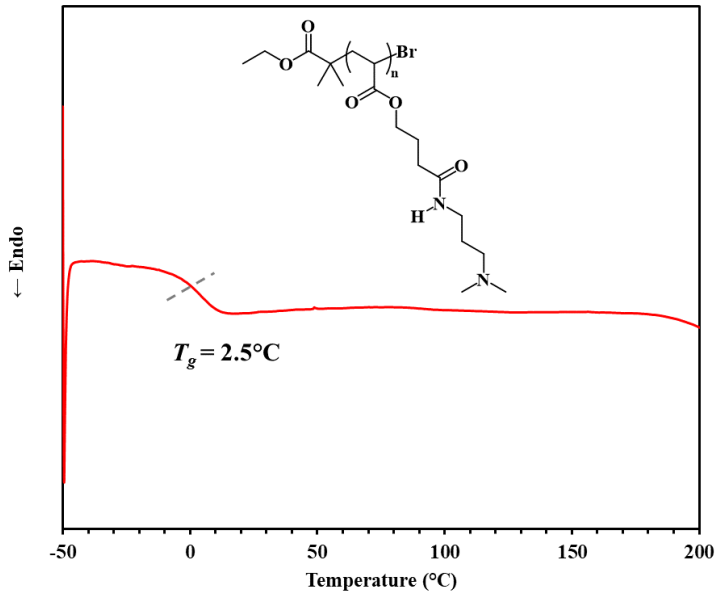

Figure S10. DSC thermogram of poly(HAAC4) synthesized by SET-LRP.

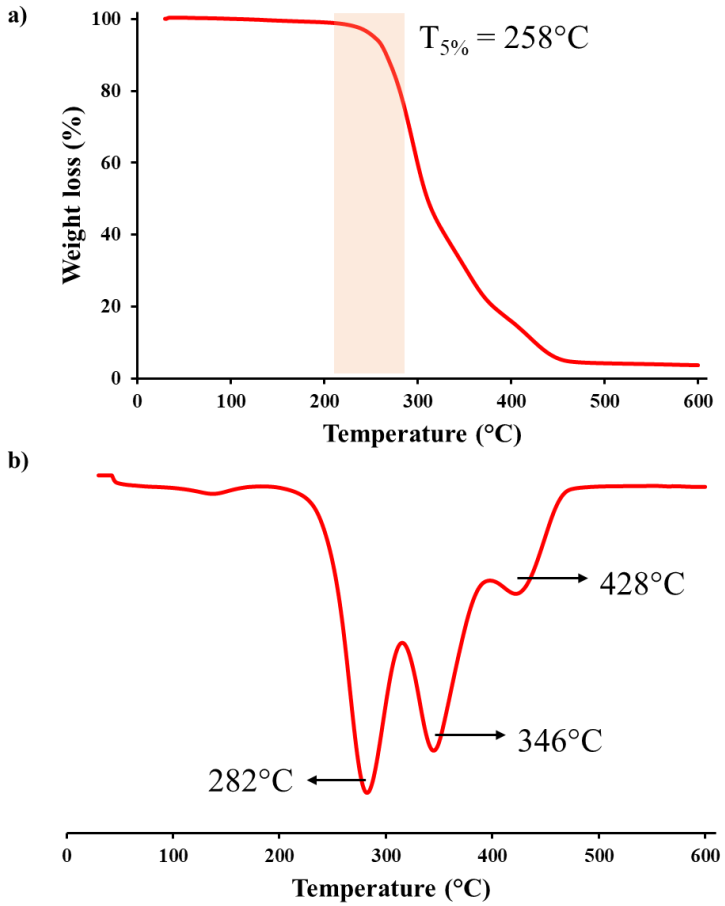

Figure S11. a) TGA analysis and b) DTGA analysis of poly(HAAC4) synthesized by SET-LRP.

Structural Characterization of Poly(BA-b-HAAC4) Block Copolymer

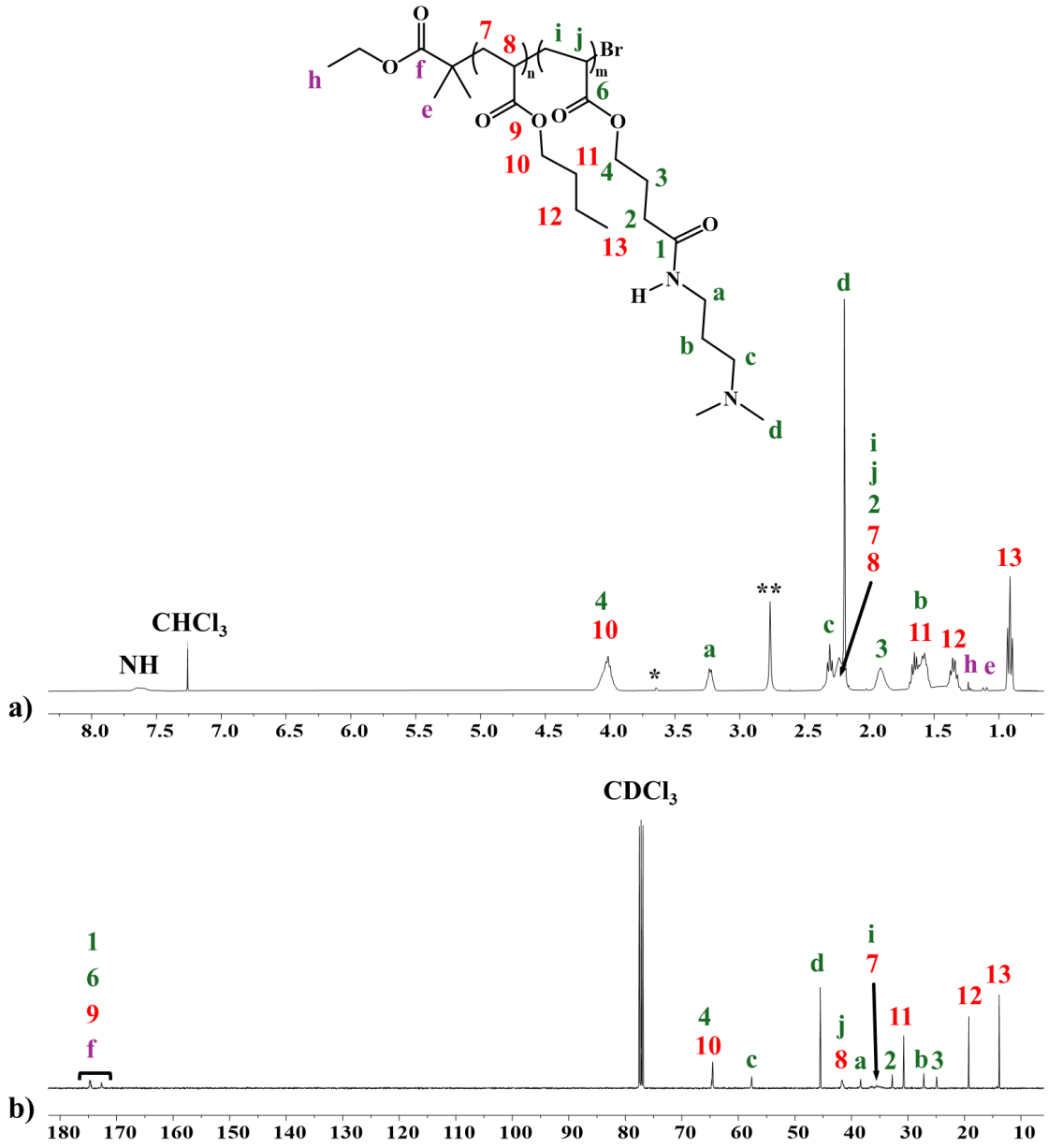

* poly(MA) traces

** H_2O traces

Figure S12. a) ^{1}H and b) ^{13}C spectra of poly(BA-*b*-HAAC4) recorded in $CDCl_3$.

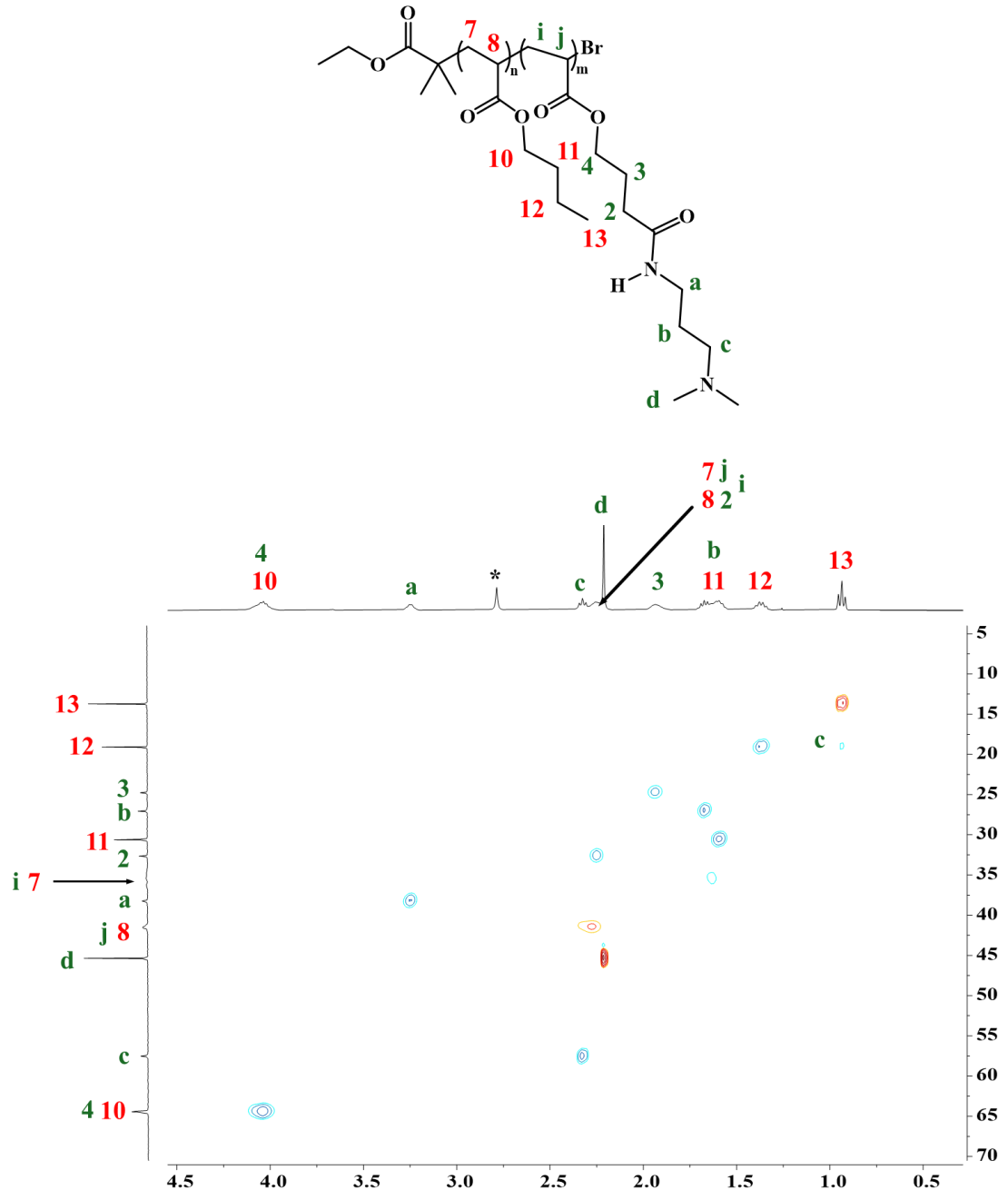

* H_2O traces

Figure S13. GHSQC correlation spectrum of poly(BA-*b*-HAAC4) recorded in $CDCl_3$.

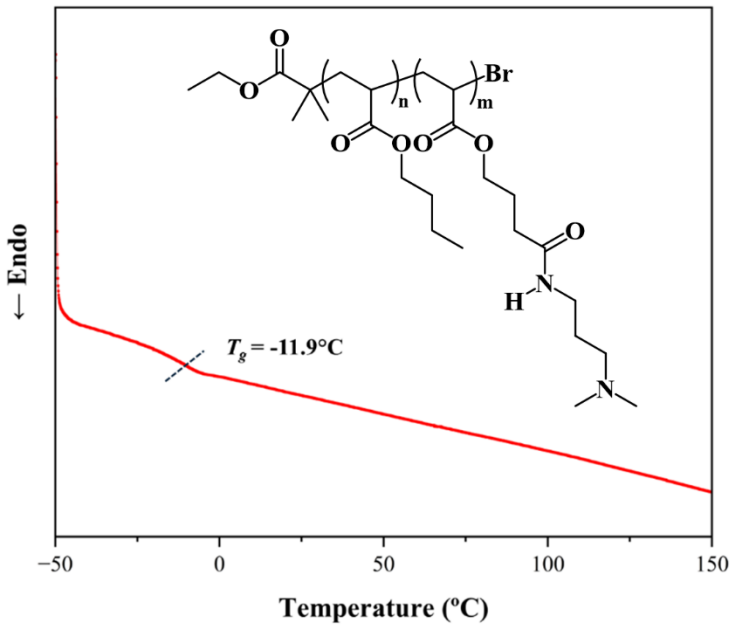

Figure S14. DSC thermogram of poly(BA-*b*-HAAC4) synthesized by SET-LRP.

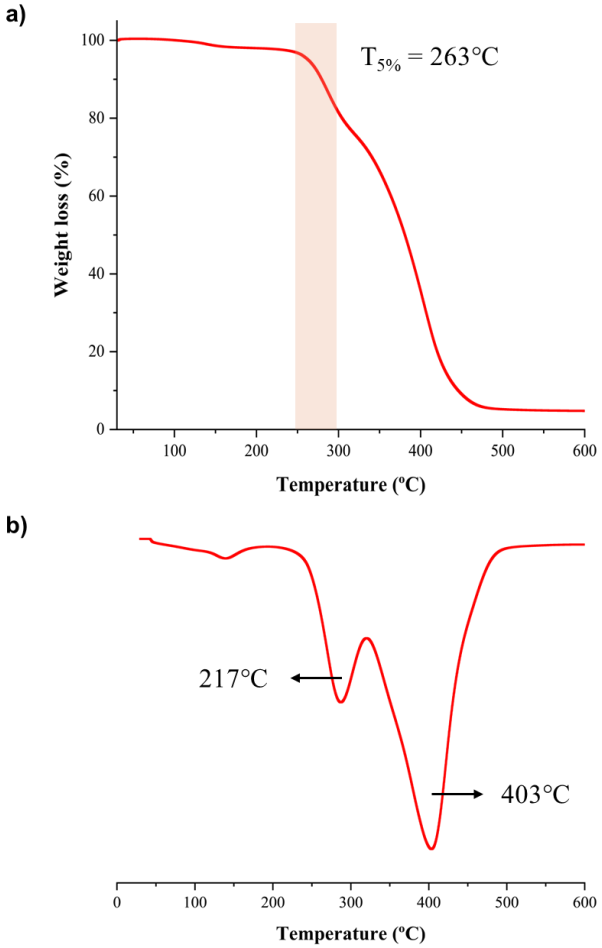

Figure S15. a) TGA analysis and b) DTGA analysis of poly(BA-*b*-HAAC4) synthesized by SET-LRP.

Structural Characterization of *N*-Ox-HAAC4

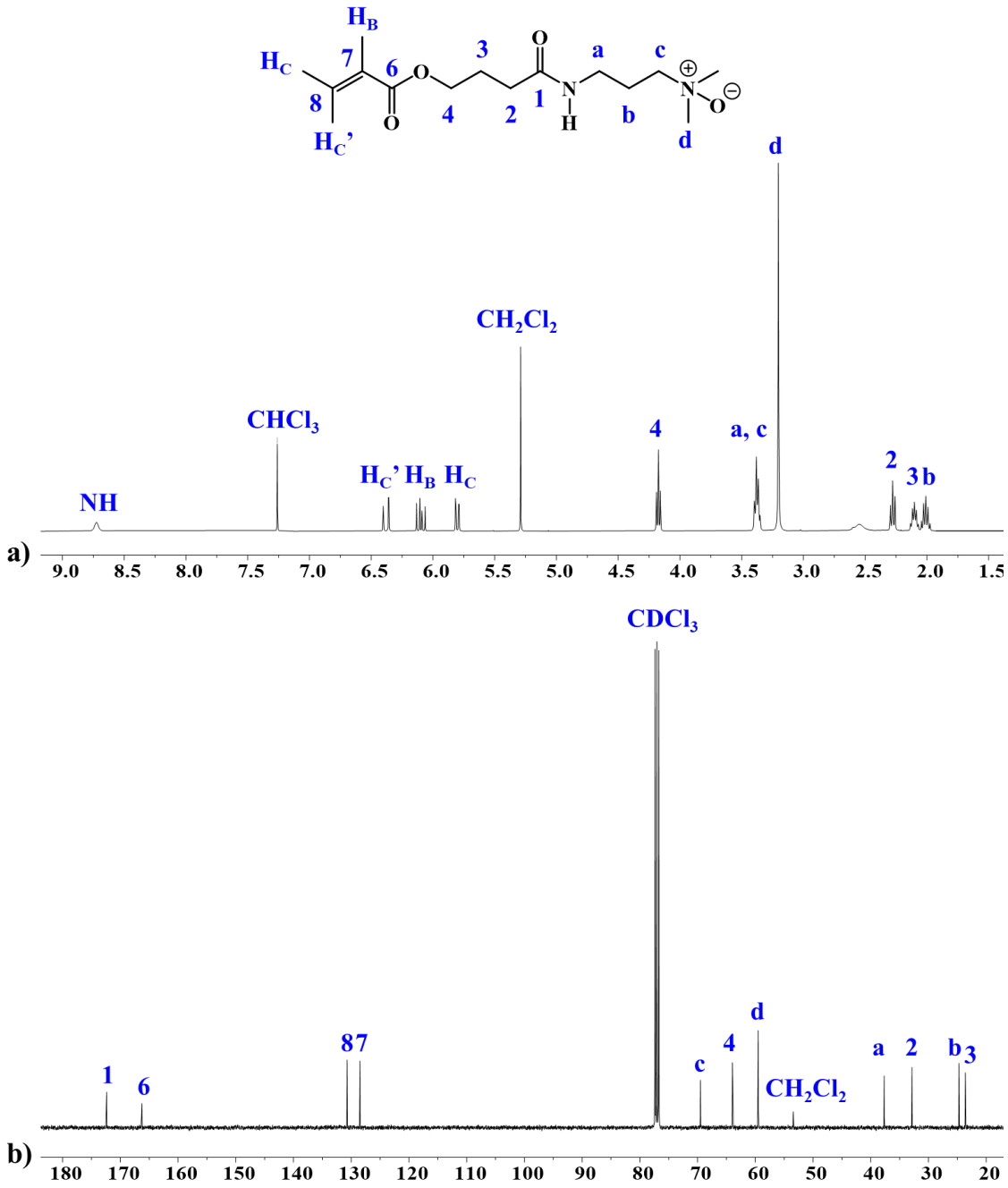

Figure S16. a) ^{1}H and b) ^{13}C NMR spectra of *N*-OX-HAAC4 recorded in $CDCl_3$.

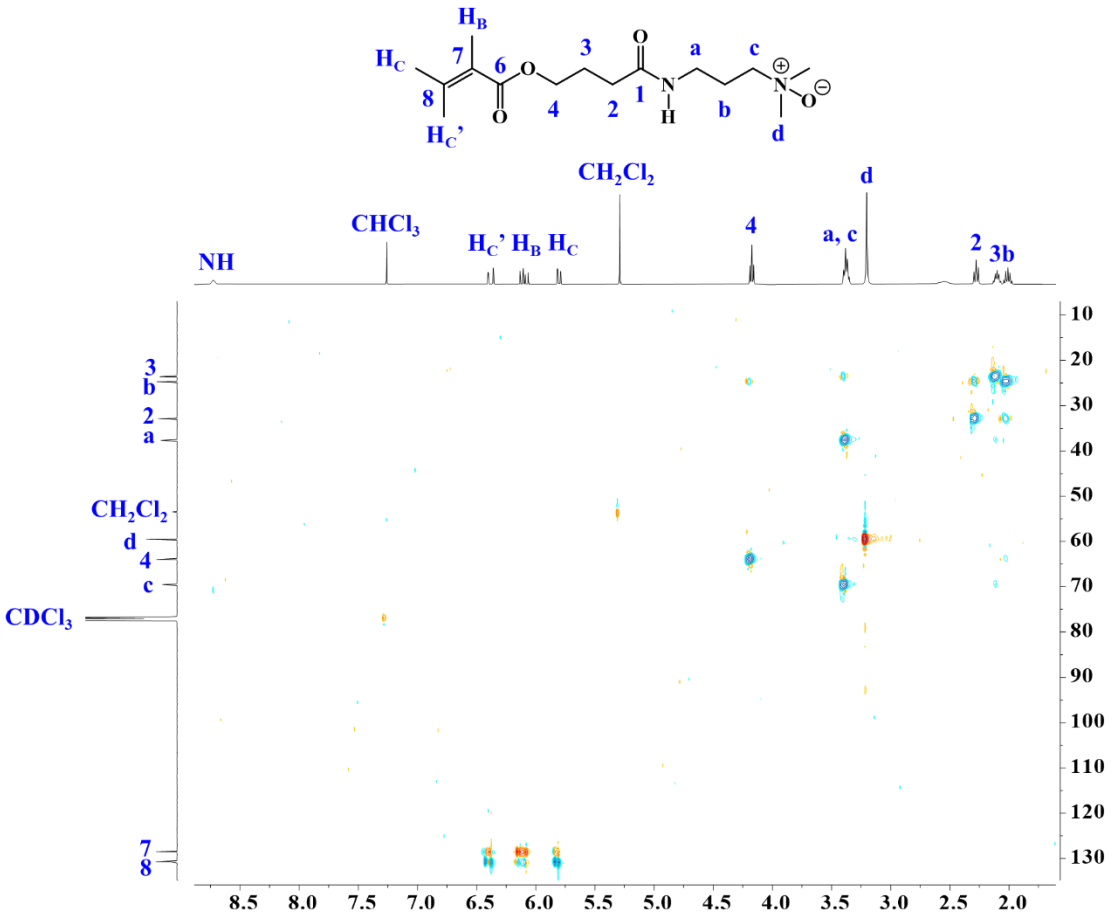

Figure S17. GHSQC correlation spectrum of *N*-Ox-HAAC4 recorded in $CDCl_3$.

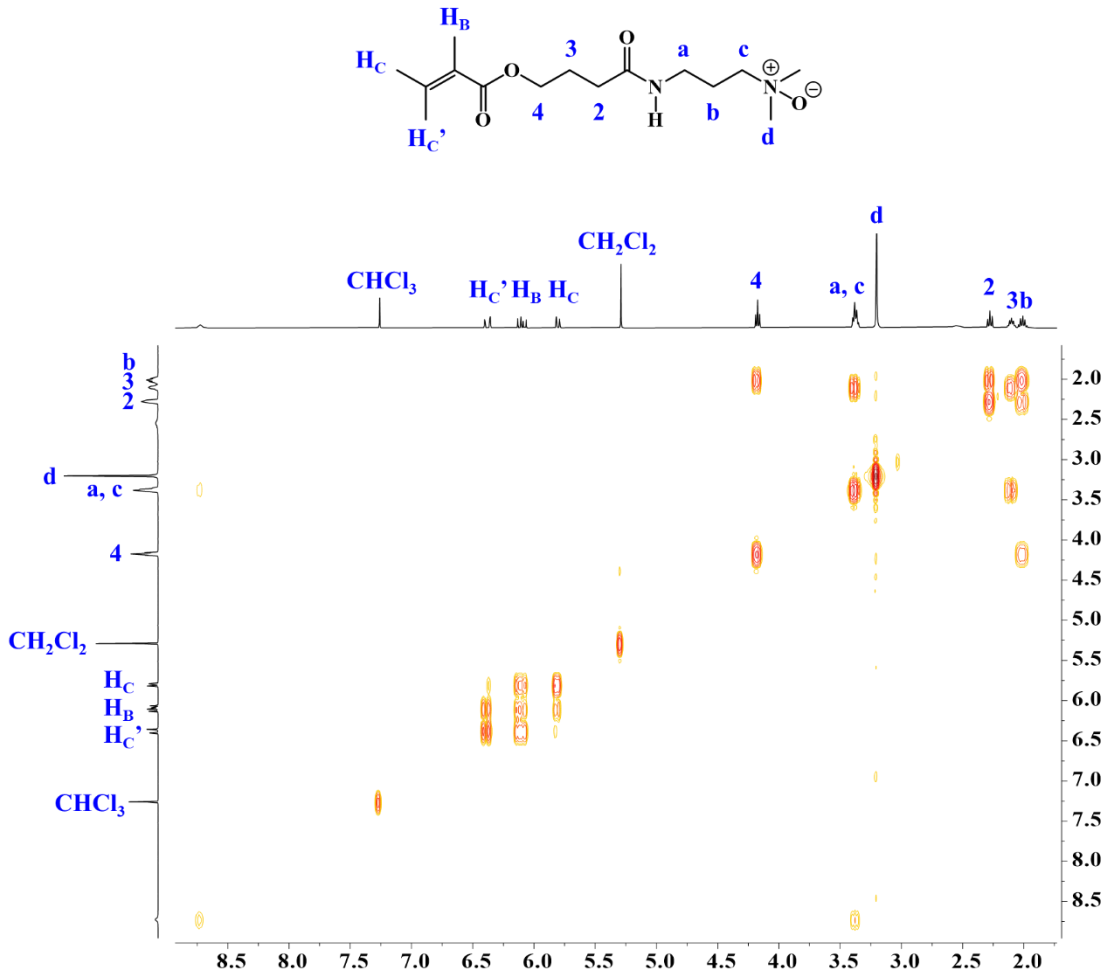

Figure S18. COSY correlation spectra of *N*-Ox-HAAC4 recorded in $CDCl_3$.